Consortium

for

Small–Scale Modelling

Technical Report No. 6

Documentation of the Z-Coordinate Dynamical Core of LM

by

H.-W. Bitzer and J. Steppeler

April 2004

DOI: 10.5676/DWD_pub/nwv/cosmo-tr_6

Deutscher Wetterdienst

MeteoSwiss

Ufficio Generale per la Meteorologia

Hellenic National Meteorological Service

Amt für Wehrgeophysik

Il Servicio Meteorologico Regionale di ARPA

www.cosmo-model.org

Editors: G. Doms and U. Schättler, Deutscher Wetterdienst, P.O. Box 100465, 63004 Offenbach, Germany
Printed at Deutscher Wetterdienst, Offenbach am Main

A Description of the Z-Coordinate Dynamical Core of LM

Heinz-Werner Bitzer and Jürgen Steppeler

Deutscher Wetterdienst, Offenbach am Main, Germany

Table of Contents

1 Introduction **1**

2 Basic Numerical Concept **2**

2.1 Equations of Motion 2

2.2 Volume Elements and Grid Design 4

2.3 Computation of Sub-Surface Values of Meteorological Fields 7

2.4 Spatial Discretization 11

3 Time Integration and Numerical Solution **14**

3.1 Fast Tendencies 14

3.2 Method of Solution 17

3.3 Structure of the Tridiagonal Matrix 20

4 Numerical Smoothing **21**

4.1 Horizontal Diffusion 21

4.2 Vertical Diffusion 24

5 Results for Idealized Test Cases **26**

6 Summary **28**

References **30**

Appendix **31**

1 Introduction

Nonhydrostatic models using terrain-following coordinates, such as the Penn State-NCAR Mesoscale Model "MM5" (Dudhia, 1993) or the Lokal-Modell "LM" (Steppeler et al., 2002) are not well suited for predictions of flow near mountains in the environment of a stratified atmosphere. Numerical errors can be induced around steep slopes, due to numrical errors in connection with the terrain following coordinate transformation. The stratified atmosphere generates artificial forces, caused by numerical errors. These can produce artificial circulations which destroy clouds in the vicinity of mountains. For example, in the model LM, the condition that such numerical forces remain reasonably small is $\delta h < dz$, with δz being the layer thickness and δh the change of orography between one gridpoint and the next. This condition is violated in most operational models, even for larger scale operational hydrostatic applications. With fine meshes the model orography tends to be steeper than for coarser meshes. Therefore the circulations driven by numerical errors can be substantial (Sundqvist, 1976).

For models using the terrain following coordinate, such as MM5 or LM, a spatially homogeneous reference profile is introduced, in order to reduce this effect. If this reference profile is rather near to the real state of the atmosphere in the model, the error mentioned is absent, and nearly perfect simulations of gravitational waves can be done. This is the situation investigated in this paper. As in addition rather smooth grid representations of the mountain are used, the terrain following coordinate can be supposed to simulate these tests very well. For operational applications on large areas it will not be possible to choose a horizontally homogeneous atmospheric reference state in the way indicated. Therefore operational applications will always suffer from numerically generated artificial forces near mountains.

A method to reduce this error has been proposed by Mesinger (1988). This method reduces the coordinate deformation by having the model layers not following the mountains, but rather ending at mountains. The lower boundary is treated under the assumption that it is represented by a step function. While this coordinate has the expected advantages in low wind situations, it has disadvantages concerning the flow around smooth topography. In particular, Gallus and Klemp (2000) reported a failure to produce proper mountain induced gravitational waves. As opposed to this, the test case proposed by Gallus and Klemp (2000) is simulated properly using the terrain following coordinate. Another z-coordinate approach was proposed by Tripoli (private communication). It has been presented at the Third International Workshop on Non-Hydrostatic Modelling in Offenbach, 1999, and does not suffer from the problems mentioned above. A short report on the workshop is given by Saito (2001). The method by Tripoli is based on posing lower boundary values for the velocity components using assumptions on the vorticity. In the present paper a different method is used to obtain the approximation near the lower boundary. The free slip boundary condition is used and numerically evaluated using the finite volume approximation.

With simple equations a sufficient convergence condition is met when the domain boundary is a continuous spline. Such a condition is present in the z-coordinate atmospheric model described here, being based on the shaved element method, used in computational fluid dynamics and oceanography (Adcroft, 1997). A cartesian structured grid corresponding to the case without orography is assumed and the topography is assumed to be represented by a bilinear spline with nodes at the gridpoints with half values of the x-axis. There are three types of grid squares: those which are completely under the earth, those completely above the topography and those which are cut by the topography function. The first two classes of elements can be treated in an obvious way. The volumes which are cut by the orography are treated by the finite volume method.

Without further approximations this method may require very small time steps, since the elements cut from a volume may be rather small. One solution would be to use a semi-implicit discretization (Thomas et al., 2000). Here we use the time splitting method, as introduced by Klemp and Wilhelmson (1978b). This has been shown by Saito (1998) to have good operational efficiency with the model LM. The problem of a restrictive CFL criterion with small cut off elements is solved by using the thin wall aproximation, which is common in oceanography. An atmospheric use of this method was tested by Bonaventura (2000). The derivation of this method from the shaved element approach requires in addition to the vertical walls also the use of horizontal walls as opposed to Bonaventura (2000), who uses vertical walls only. Test integrations using this method in two space dimensions will be given in Section 3. The test problems proposed by Gallus and Klemp (2000) are simulated properly by the z-coordinate version of LM.

The present paper gives an extensive description of the z-coordinate, as implemented in the LM. THe tests involving an idealized bell shaped mountain are described. They perform well and the z-coordinate LM is now ready for further development towards operational implementation.

2 Basic Numerical Concept

2.1 Equations of Motion

The following numerical model simulates a 3d atmospheric flow in z-coordinates. Since the z-surfaces are horizontal, the governing equations are formulated in an orthogonal coordinate system on a sphere. The underlying mathematical structure consists of the full compressible Euler equations. The model takes gravity, coriolis force and metric terms into account, Reynolds stresses and viscosity are neglected. Physical processes like cloud physics, radiation and boundary layer physics are not included. The current version is suitable for idealized experiments in fluid flows and is the starting point to develop a weather forecast model in a z-coordinate system. The equations are the same as for the operational LM (Doms and Schaettler 2001) with the simplifications mentioned above. The equations read:

$$\frac{\partial u}{\partial t} = -\vec{v}\cdot\nabla u + \frac{uv}{a}\tan\varphi + fv - \frac{1}{\rho a\cos\varphi}\frac{\partial p}{\partial\lambda} \tag{1}$$

$$\frac{\partial v}{\partial t} = -\vec{v}\cdot\nabla v - \frac{u^2}{a}\tan\varphi - fu - \frac{1}{\rho a}\frac{\partial p}{\partial\varphi} \tag{2}$$

$$\frac{\partial w}{\partial t} = -\vec{v}\cdot\nabla w - \frac{1}{\rho}\frac{\partial p}{\partial z} - g \tag{3}$$

$$\frac{\partial p}{\partial t} = -\vec{v}\cdot\nabla p - \frac{c_p}{c_v}pD_3 \tag{4}$$

$$\frac{\partial T}{\partial t} = -\vec{v}\cdot\nabla T - \frac{1}{\rho c_v}pD_3 \tag{5}$$

The advection operator is definied by

$$\vec{v}\cdot\nabla = \frac{1}{a\cos\varphi}\left(u\frac{\partial}{\partial\lambda} + v\cos\varphi\frac{\partial}{\partial\varphi}\right) + w\frac{\partial}{\partial z} \tag{6}$$

and the threedimensional wind divergence by

$$D_3 = \frac{1}{a\cos\varphi}\left[\frac{\partial u}{\partial\lambda} + \frac{\partial}{\partial\varphi}(v\cos\varphi)\right] + \frac{\partial w}{\partial z} \tag{7}$$

The vertical acceleration due to the pressure gradient and gravity in (1.3) is expanded as

$$-\frac{1}{\rho}\frac{\partial p}{\partial z} - g = g\frac{\rho_0}{\rho}\left(\frac{T-T_0}{T} - \frac{T_0}{T}\frac{p'}{p_0}\right) - \frac{1}{\rho}\frac{\partial p'}{\partial z} \tag{8}$$

p' is the predicted pressure perturbation. p is the total pressure calculated as the sum of base-state pressure and predicted pressure perturbation:

$$p = p_0 + p' \tag{9}$$

The full set of model equations become

$$\frac{\partial u}{\partial t} = -\vec{v}\cdot\nabla u + \frac{uv}{a}\tan\varphi + fv - \frac{1}{\rho a\cos\varphi}\frac{\partial p'}{\partial\lambda} \tag{10}$$

$$\frac{\partial v}{\partial t} = -\vec{v}\cdot\nabla v - \frac{u^2}{a}\tan\varphi - fu - \frac{1}{\rho a}\frac{\partial p'}{\partial\varphi} \tag{11}$$

$$\frac{\partial w}{\partial t} = -\vec{v}\cdot\nabla w + g\frac{\rho_0}{\rho}\left[\frac{T-T_0}{T} - \frac{T_0}{T}\frac{p'}{p_0}\right] - \frac{1}{\rho}\frac{\partial p'}{\partial z} \tag{12}$$

$$\frac{\partial p'}{\partial t} = -\vec{v}\cdot\nabla p' + g\rho_0 w - \frac{c_p}{c_v}pD_3 \tag{13}$$

$$\frac{\partial T}{\partial t} = -\vec{v}\cdot\nabla T - \frac{1}{\rho c_v}pD_3 \tag{14}$$

The governing nonhydrostatic equations describe a compressible model atmosphere, thus meteorological unimportant sound waves are also part of the solution. According to the Courant Friedrich Levy criterion the fastest signal velocity, i.e. the sound velocity, determines the integration time step. In order to keep numerical efficiency, the mode-splitting time-integration method proposed be Klemp and Wilhelmson (1978) is applied. In practice the mode splitting time integration scheme in symbolic form can be written as:

$$\frac{\partial\psi}{\partial t} = s_\psi + f_\psi \tag{15}$$

Where ψ denotes a prognostic model variable, f_ψ the forcing terms due to the slow modes and s_ψ the source terms which are related to the acoustic and gravity wave mode (fast mode).

The full set of model equations can then be split:

a) slow tendencies

$$f_u = -\vec{v}\cdot\nabla u + \frac{uv}{a}\tan\varphi + fv \tag{16}$$

$$f_v = -\vec{v}\cdot\nabla v - \frac{u^2}{a}\tan\varphi - fu \tag{17}$$

$$f_w = -\vec{v}\cdot\nabla w \tag{18}$$

$$f_{p'} = -\vec{v}\cdot\nabla p' \tag{19}$$

$$f_T = -\vec{v}\cdot\nabla T \tag{20}$$

b) fast tendencies:

$$s_u = -\frac{1}{\rho a \cos\varphi}\frac{\partial p'}{\partial \lambda} \quad (21)$$

$$s_v = -\frac{1}{\rho a}\frac{\partial p'}{\partial \varphi} \quad (22)$$

$$s_w = -\frac{1}{\rho}\frac{\partial p'}{\partial z} + g\frac{\rho_0}{\rho}\left[\frac{T-T_0}{T} - \frac{T_0}{T}\frac{p'}{p_0}\right] \quad (23)$$

$$s_{p'} = g\rho_0 w - \frac{c_p}{c_v} pD_3 \quad (24)$$

$$s_T = -\frac{1}{\rho c_v} pD_3 \quad (25)$$

The f_ψ -terms denote the tendencies due to the slow modes. These terms are kept constant during the subcycle procedure. The equations for w' p' and T are coupled and solved implicitly.

Currently the model still runs with the originally introduced $\Delta\,(p_0)_k$ (thickness of layer k expressed by Δp_0) which is present in the entire programm code. So the vertical derivative is written as:

$$\frac{\partial}{\partial z} = -\frac{g\rho_0}{\Delta p_0}\frac{\partial}{\partial \zeta} \quad (26)$$

2.2 Volume Elements and Grid Design

The Arakawa C-Grid of the LM is used in the current model. Fig. 2.1 illustrates the staggering of the dependent model variables.

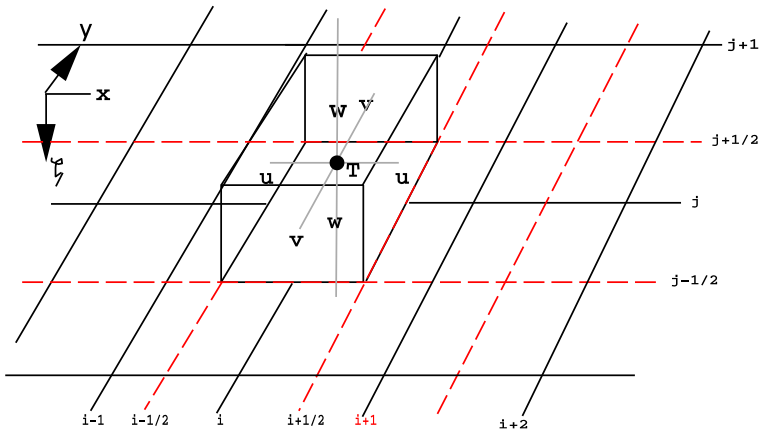

FIGURE 2.1: The three dimensional grid box.

Note, that the ζ -coordinate in the vertical is still used with $\Delta\zeta = 1$. Eq. (1.26) is applied to gain $\frac{\partial}{\partial z}(...)$.

The orography is definied at the corner points $(i+1/2, j+1/2)$ of a grid element (see Fig. 2.2).

Fig. 2.3 illustrates, how the surface of the orography intersects a column of volume elements.

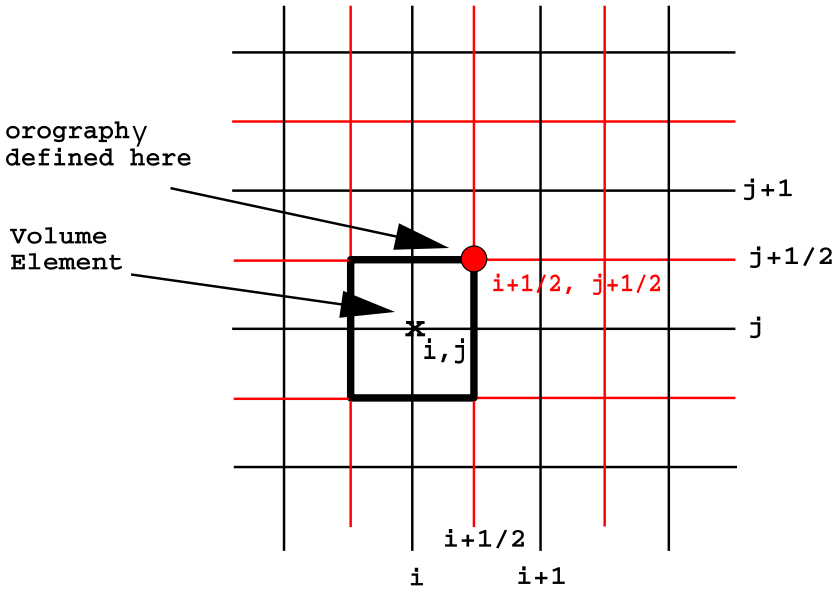

FIGURE 2.2: The horizontal grid and the definition of orography.

Fig. 2.4 illustrates for a bell shaped mountain, how the mountain's surface intersects the volume element. In the LM with terrain-following coordinates the horizontal pressure gradient is gained by applying the transformation formula which takes the vertical pressure difference along the sloped surface into account. Since the current model is formulated in z-coordinates, we have no metric term in the expression for (see Doms and Schättler, 2001) $\frac{\partial p}{\partial x}$ is not longer present. Instead a significant difference in the calculation of the spatial derivatives between the current model and the LM appears. As shown in Fig. 1.4 the volume element located at i, j, k is cut by the mountain's surface. In the advection term of equation (1.16),

$$-\vec{v}\cdot\nabla u = \underbrace{-u\frac{\partial u}{\partial x}}_{1} - v\frac{\partial u}{\partial y} - w\frac{\partial u}{\partial z} \tag{27}$$

the three terms have to be determined at position $i+1/2, j, k$. For term 1 this is done in the following way, using the centered difference approximation

$$-u\frac{\partial u}{\partial x} = \overline{-\overline{u}^{x}\frac{\partial u}{\partial x}}^{x} = -\frac{1/2}{\Delta x}\left(u_{i,j,k}\Delta u_{i,j,k} + u_{i+1,j,k}\Delta u_{i+1,j,k}\right) \tag{28}$$

$$\text{with } u_{i,j,k} = \frac{1}{2}\left(u_{i-1/2,j,k} + u_{i+1/2,j,k}\right) \tag{29}$$

$$\Delta u_{i,j,k} = u_{i+1/2,j,k} - u_{i-1/2,j,k} \tag{30}$$

$$\Delta u_{i+1/j,k} = u_{i+11/2,j,k} - u_{i+1/2,j,k} \tag{31}$$

The velocity $u_{i-1/2,j,k}$ required in (1.29) and (1.30) which is denoted in Fig. 2.4 with u^*, is unknown, as it is underneath the mountain.

Fig. 2.5 gives a horizontal cross section through the grid. All values within the dashed area (see Fig. 2.5) lie underneath the mountain's surface. The solid line represents the

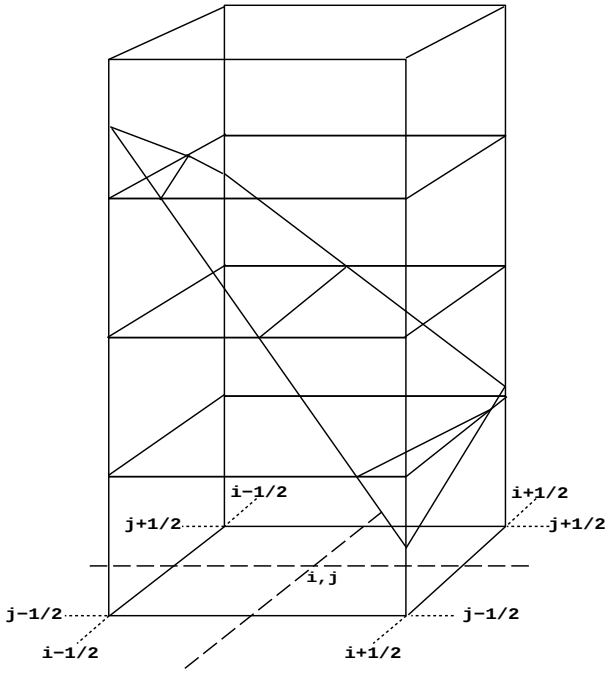

FIGURE 2.3: A column and the cells cut by a bilinear function representing the orography.

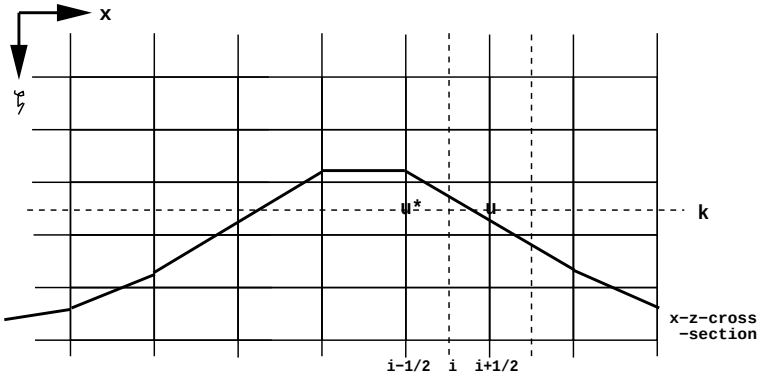

FIGURE 2.4: A vertical cross section through the grid and the boundary value u^* under the mountain.

intersection curve of the mountain's surface and a z-plane. Applying the formula

$$-v\frac{\partial u}{\partial y} = \overline{-\overline{v}^x \frac{\partial u}{\partial y}}^y = -\frac{1/2}{\Delta y}\left(v_{i+1/2,j+1/2,,k}\Delta u_{i+1/2,j+1/2,k} + v_{i+1/2,j-1/2,k}\Delta u_{i+1/2,j-1/2,k}\right) \quad (32)$$

with

$$v_{i+1/2,j-1/2,k} = \frac{1}{2}\left(\underline{v_{i,j-1/2,k}} + v_{i+1,j-1/2,k}\right) \quad (33)$$

and

$$\Delta u_{i+1/2,j-1/2,k} = u_{i+1/2,j,k} - \underline{u_{i+1/2,j-1,k}} \quad (34)$$

$v_{i,j-1/2,k}$ and $u_{i+1/2,j-1,k}$ are unknown quantities under the mountain. Our goal is, to determine a realistic value for $-u\frac{\partial u}{\partial x}$ and $-v\frac{\partial u}{\partial y}$ at point $i+1/2, j, k$. In order to do that the star values are computed.

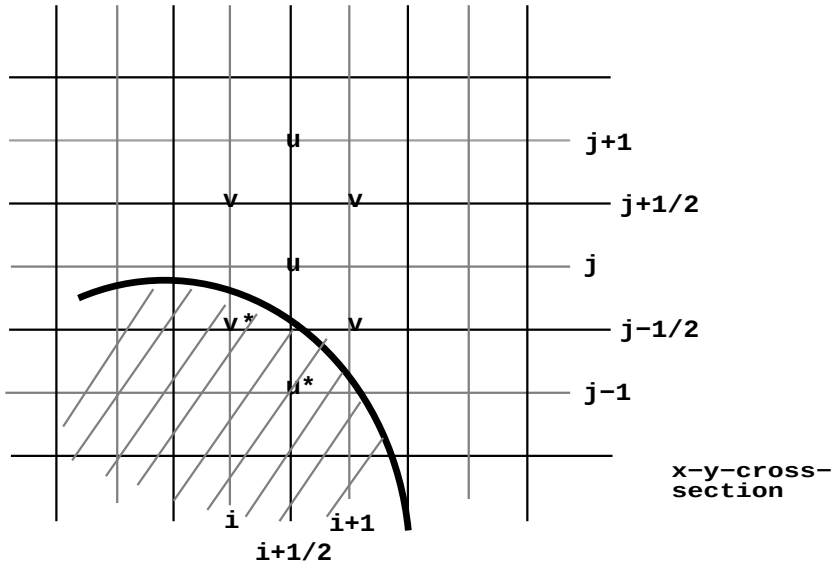

FIGURE 2.5: A horizontal cross section through the grid with boundary values in the horizontal

Please note, the star values are not computed in order to gain realistic values under the mountain. These quantities are artificial. The star values are just preliminary values, so called help values which are necessary to compute a realistic derivative at a point which lies very close at the boundary. In the horizontal plane (Fig. 2.5) the star quantities are those, which have at least one neighbour in the same plane positioned in the free atmosphere.

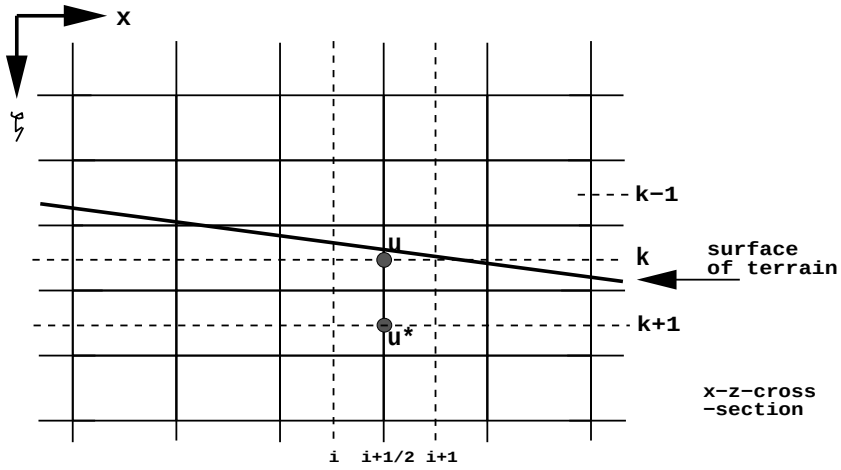

FIGURE 2.6: Boundary values u^* under flat terrain.

In many cases the surface of the terrain is flat (see Fig. 2.6). A star value under the surface is necessary for the correct evaluation of the vertical derivative. As illustrated in Fig. 2.6 u^* at $i+1/2, j, k+1$ is required for $\left.\frac{\partial u}{\partial \zeta}\right|_{i+1/2,j,k+1/2}$.

2.3 Computation of Sub-Surface Values of Meteorological Fields

The situation is represented in Fig. 2.7 where u^* as a help quantity has to be evaluated. In the current model a three point formula is applied.

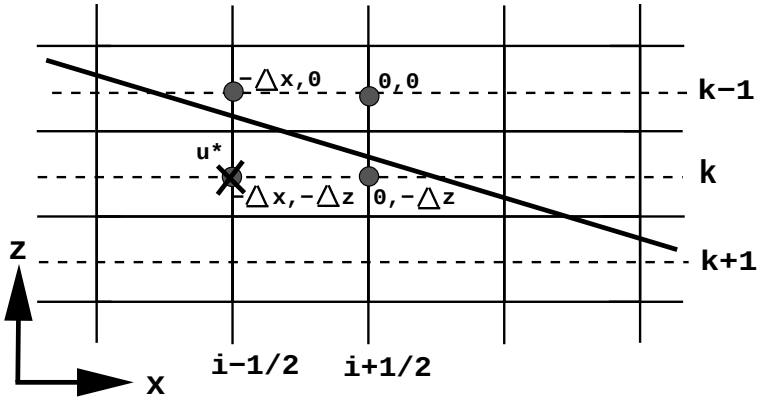

FIGURE 2.7: The interpolation of sub-surface boundary values $u^*$from surrounding values u.

Since the curvature of the spatial distribution of u is not taken into account the three points have to be chosen very close to the boundary. The method to yield u^* is based on the formula for a plane in a 3-dimensional space.

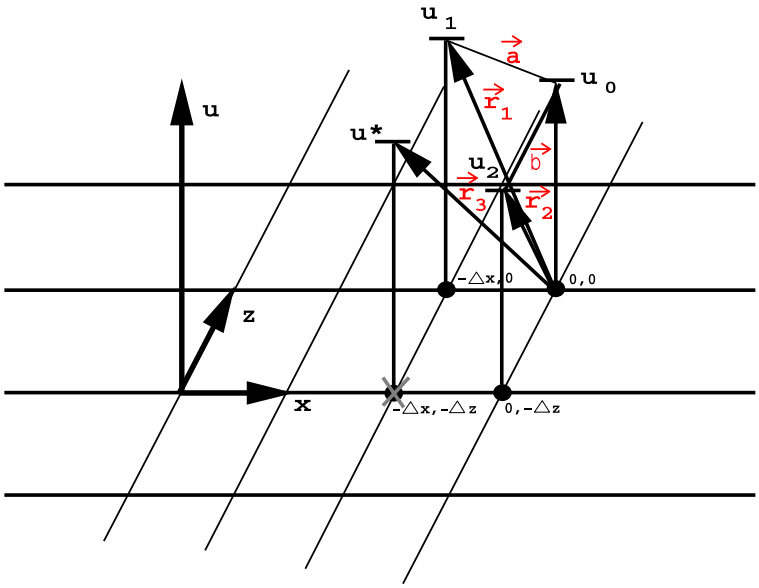

FIGURE 2.8: The plane used for the interpolation of u^*.

The plane is stretched by the vectors $\vec{a}$ and $\vec{b}$ in Fig. 2.8. The origin of the relative coordinate system is detoned with 0,0. The vectors $\vec{r_0}, \vec{r_1}, \vec{r_2}$ and $\vec{r_3}$ are the position vectors pointing to u_0, u_1, u_2 and u^*, they read:

$$\vec{r_0} = \begin{pmatrix} 0 \\ 0 \\ u_0 \end{pmatrix} ; \vec{r_1} = \begin{pmatrix} -\Delta x \\ 0 \\ u_1 \end{pmatrix} ; \vec{r_2} = \begin{pmatrix} 0 \\ -\Delta z \\ u_2 \end{pmatrix} ; \vec{r_3} = \begin{pmatrix} -\Delta x \\ -\Delta z \\ u_* \end{pmatrix} \tag{35}$$

The general formula of a plane in parameter representation is:

$$\vec{r} = \vec{r_0} + \lambda\vec{a} + \mu\vec{b} \tag{36}$$

where λ and μ are the parameters and $\vec{r}$ is a vector pointing to a point in the plane which

is stretched by $\vec{a}$ and $\vec{b}$. $\vec{a} = \vec{r_1} - \vec{r_0}$; $\vec{b} = \vec{r_2} - \vec{r_0}$ from (1.35) follows:

$$\vec{a} = \begin{pmatrix} -\Delta x \\ 0 \\ u_1 - u_0 \end{pmatrix} \quad ; \quad \vec{b} = \begin{pmatrix} 0 \\ -\Delta z \\ u_2 - u_0 \end{pmatrix} \tag{37}$$

The demand is: u^* is located within the plane. Thus, vector $\vec{r}$ in (1.36) can be replaced by $\vec{r_3}$:

$$\begin{pmatrix} -\Delta x \\ -\Delta z \\ u^* \end{pmatrix} = \begin{pmatrix} 0 \\ 0 \\ u_0 \end{pmatrix} + \lambda^* \begin{pmatrix} -\Delta x \\ 0 \\ u_1 - u_0 \end{pmatrix} + \mu^* \begin{pmatrix} 0 \\ -\Delta z \\ u_2 - u_0 \end{pmatrix} \tag{38}$$

The first two components of the vector equation (1.37) represent a linear system of equations for the unknowns λ^* and μ^*. The result is $\lambda^* = 1$, $\mu^* = 1$. For u^* we find the relation:

$$\begin{aligned} u^* &= u_0 + (u_1 - u_0) + (u_2 - u_0) \Rightarrow \\ u^* &= u_1 + u_2 - u_0 \end{aligned} \tag{39}$$

$$\begin{aligned} \text{substituting} \quad u^* &= u_{i-1/2,j,k} \\ u_1 &= u_{i-1/2,j,k-1} \\ u_2 &= u_{i+1/2,j,k} \\ u_0 &= u_{i+1/2,j,k-1} \qquad \text{yields} \qquad (40) \\ u_{i-1/2,j,k} &= u_{i-1/2,j,k-1} + u_{i+1/2,j,k} - u_{i+1/2,j,k-1} \qquad (41) \end{aligned}$$

(1.41) is the answer for the preliminary value $u_{i-1/2,j,k}$ in case that the mountain is on the west side. For the other sides the formula looks very similar.

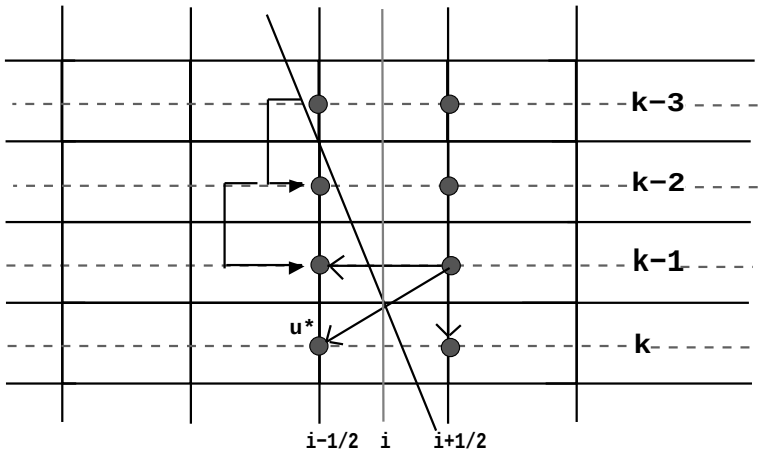

FIGURE 2.9: The interpolation in case of a steep mountain going from top to bottom.

Fig. 1.9 illustrates the situation in case of a steep slope. Applying (1.28) would fail for u^* if the calculation were started from below because $u_{i-1/2,j,k-1}$ is also unknown. Since the calculation procedure starts from upper levels downward, first $u_{i-1/2,j,k-1}$ is calculated because $u_{i-1/2,j,k-2}$ is available and finally u^* at k can be computed. In case of a flat terrain

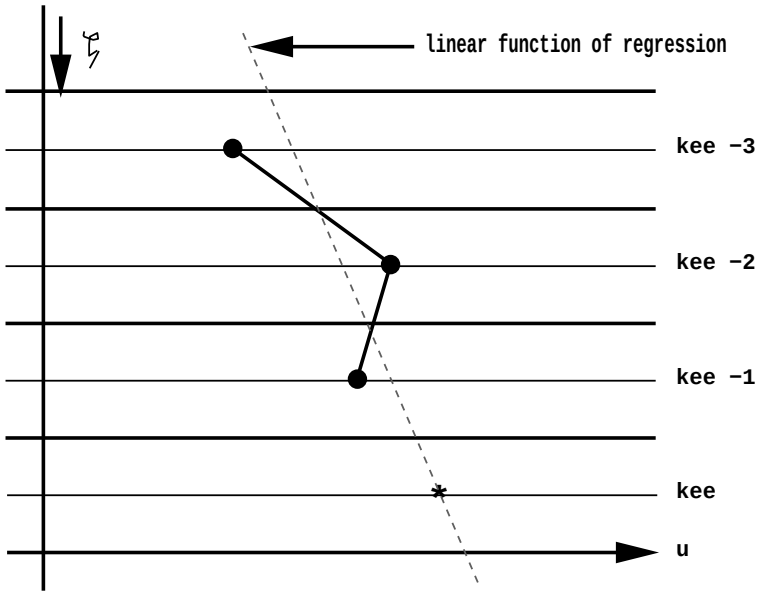

FIGURE 2.10: The linear regression used near the surface.

(Fig. 2.6) instead of the formula of a plane, a one dimensional linear function of regression is applied to compute u^*.

Let's assume that kee in Fig. 2.10 is the first level under the terrain with respect to the ζ-direction. Then $u_{i+1/2,j,kee-1}$, $u_{i+1/2,,j,kee}$ and $u_{i+1/2,j,kee-3}$ are taken to determine the linear function of regression:

$$
\begin{aligned}
u^*_{i+1/2,j,kee} &= um + 2us \qquad (42)\\
&\text{with}\\
um &= \frac{1}{3}\left(u_{i+1/2,j,kee-3} + u_{i+1/2,j,kee-2} + u_{i+1/2,j,kee-1}\right)\\
&\text{and}\\
us &= \frac{u_{i+1/2,j,kee-1} - u_{i+1/2,j,kee-3}}{2\Delta\zeta}\\
\text{because} \quad \Delta\zeta &= 1 \quad \text{yields:}\\
us &= \frac{1}{2}\left(u_{i+1/2,j,kee-1} - u_{i+1/2,j,kee-3}\right)
\end{aligned}
$$

The preliminary star values of the other parameters are computed in the same way. Finally, all the necessary star values are processed and all the derivatives close to the boundary can be determined. The calculation procedure can be done in a subroutine which is called in the model before the slow tendencies are calculated. The advantage of this program structure is: no if statement is necessary while the slow tendencies are processed. At all the other gridpoints under the surface the field is filled with 0. For the calculation procedure they don't have any importance. In fact they must not have any importance. The program can be tested by writing strange numbers under the surface (except the star values). They should not have any impact on the solution of the flow field. Do loops in i-, j- and k-direction don't need to be interrupted at the boundaries. This is important in order to keep the integration sweeps in x-, y- and z-direction efficient.

2.4 Spatial Discretization

To present the difference form of equations (1.16)-(1.25) the following notations for horizontal and vertical averaging and differencing are defined.

$$
\begin{aligned}
\overline{\psi}^{\lambda} &= \frac{1}{2}\left(\psi\left(\lambda+\frac{\Delta\lambda}{2}\right)+\psi\left(\lambda-\frac{\Delta\lambda}{2}\right)\right)\\
\overline{\psi}^{\varphi} &= \frac{1}{2}\left(\psi\left(\varphi+\frac{\Delta\varphi}{2}\right)+\psi\left(\varphi-\frac{\Delta\varphi}{2}\right)\right)\\
\overline{\psi}^{m\zeta} &= \frac{1}{2}\left(\psi_{k+1/2}+\psi_{k-1/2}\right)\\
\overline{\psi}^{h\zeta}_{k-1/2} &= \frac{\Delta\left(p_0\right)_{k-1}\psi_k+\Delta\left(p_0\right)_k\psi_{k-1}}{\Delta\left(p_0\right)_{k-1}+\Delta\left(p_0\right)_k}\\
\delta_{\lambda}\left(\psi\right) &= \psi\left(\lambda+\frac{\Delta\lambda}{2}\right)-\psi\left(\lambda-\frac{\Delta\lambda}{2}\right)\\
\delta_{\varphi}\left(\psi\right) &= \psi\left(\varphi+\frac{\Delta\varphi}{2}\right)-\psi\left(\varphi-\frac{\Delta\varphi}{2}\right)\\
\delta_{\varphi}\left(\psi\right) &= \psi\left(\zeta+\frac{1}{2}\right)-\psi\left(\zeta-\frac{1}{2}\right)
\end{aligned}
$$

The vertical advection $-w\frac{\partial\psi}{\partial z}$ is still written with the contravariant vertical velocity $\dot{\zeta}$ (see LM operational version):

$$
\begin{aligned}
-w\frac{\partial\psi}{\partial z} &= -\dot{\zeta}\frac{\partial\psi}{\partial\zeta} \qquad ; \qquad \dot{\zeta}_{k-1/2}=\frac{w^*_{k-1/2}}{\Delta\left(p_0\right)_{k-1/2}}=\frac{w_{k-1/2}}{\Delta z_{k-1/2}}\\
w^*_{k-1/2} &= -g\overline{\left(\rho_0\right)}^{h\zeta}_{k-1/2}w_{k-1/2} \qquad ; \qquad \Delta\left(p_0\right)_{k-1/2}=\frac{1}{2}\left(\Delta\left(p_0\right)_k+\Delta\left(p_0\right)_{k-1}\right)\\
\Delta z_{k-1/2} &= \frac{1}{2}\left(\Delta z_k+\Delta z_{k-1}\right)
\end{aligned}
\tag{43}
$$

With these notations the slow tendencies of (1.10) - (1.20) read:

$$
\begin{aligned}
f_u &= -\frac{1}{a\overline{\cos\varphi}^{\varphi}\Delta\lambda}\overline{\overline{u}^{\lambda}\delta_{\lambda}\left(u\right)}^{\lambda}-\frac{1}{a\overline{\cos\varphi}^{\varphi}\Delta\varphi}\overline{\overline{v}^{\lambda}\cos\varphi\delta_{\varphi}\left(u\right)}^{\varphi}\\
&\quad -\overline{\overline{\dot{\zeta}}^{\lambda}\delta_{\lambda}\left(u\right)}^{m\zeta}+\frac{u\overline{v}^{\lambda,\varphi}\overline{tan\varphi}^{\varphi}}{a}+\overline{f}^{\varphi}\overline{v}^{\lambda,\varphi}
\end{aligned}
\tag{44}
$$

$$
\begin{aligned}
f_v &= -\frac{1}{a\cos^{\varphi}\Delta\lambda}\overline{\overline{u}^{\varphi}\delta_{\lambda}\left(v\right)}^{\lambda}-\frac{1}{a\cos\varphi\Delta\varphi}\overline{\overline{v}^{\varphi}\overline{\cos\varphi}^{\varphi}\delta_{\varphi}\left(v\right)}^{\varphi}\\
&\quad -\overline{\overline{\dot{\zeta}}^{\varphi}\delta_{\zeta}\left(v\right)}^{m\zeta}-\frac{\left(\overline{u}^{\lambda,\varphi}\right)^2}{a}tan\varphi-\overline{f}^{\lambda}\overline{u}^{\lambda,\varphi}
\end{aligned}
\tag{45}
$$

$$
f_w = -\frac{1}{a\overline{\cos^{\varphi}\varphi}^{\varphi}\Delta\lambda}\overline{\overline{u}^{h\zeta}\delta_{\lambda}\left(w\right)}^{\lambda}-\frac{1}{a\overline{\cos\varphi}^{\varphi}\Delta\varphi}\overline{\overline{v}^{h\zeta}\cos\varphi\delta_{\varphi}\left(w\right)}^{\varphi}-\overline{\overline{\dot{\zeta}}^{m\zeta}\delta_{\zeta}\left(w\right)}^{m\zeta} \tag{46}
$$

$$
f'_p = -\frac{1}{a\overline{\cos^{\varphi}\varphi}^{\varphi}\Delta\lambda}\overline{u\delta_{\lambda}\left(p'\right)}^{\lambda}--\frac{1}{a\overline{\cos\varphi}^{\varphi}\Delta\varphi}\overline{v\cos\varphi\delta_{\varphi}\left(p'\right)}^{\varphi}-\overline{\dot{\zeta}\delta_{\zeta}\left(p'\right)}^{m\zeta} \tag{47}
$$

$$
f_T = -\frac{1}{a\overline{\cos^{\varphi}\varphi}^{\varphi}\Delta\lambda}\overline{u\delta_{\lambda}\left(T\right)}^{\lambda}-\frac{1}{a\overline{\cos\varphi}^{\varphi}\Delta\varphi}\overline{v\cos\varphi\delta_{\varphi}\left(T\right)}^{\varphi}-\overline{\dot{\zeta}\delta_{\varphi}\left(T\right)}^{m\zeta} \tag{48}
$$

The slow tendencies are finally multiplied by the digital factors 0 or 1 depending on whether the location of the parameter is under the surface or in the free atmosphere respectively:

$$\begin{aligned} f_{u_{i,j,k}} &= f_{u_{i,j,k}} weightu_{i,j,k} \\ f_{v_{i,j,k}} &= f_{v_{i,j,k}} weightv_{i,j,k} \\ f_{w_{i,j,k}} &= f_{w_{i,j,k}} weight_{i,j,k} \\ f_{p'_{i,j,k}} &= f_{p'_{i,j,k}} weight_{i,j,k} \\ f_{T_{i,j,k}} &= f_{T_{i,j,k}} weight_{i,j,k} \end{aligned} \tag{49}$$

The tendencies of all the parameters under the surface are zero. This implies that those parameters keep their initial value and have to be set only once. The digital factors, here denoted with *weightu*, *weightv* and *weight* are processed in a special subroutine (*z_level.f90* of *src_artifdata.f90*) at the beginning of the program run. In the program code some coefficients can be separated from equations (1.44) - (1.48):

1. horizontal advection of u and v:

$$\begin{aligned} zfadsx(j) &= \frac{1/2}{a\cos\varphi_j \Delta\lambda} \\ zfadsy(j) &= \frac{1/2}{a\cos\varphi_j \Delta\varphi} \\ zfadvx(j) &= \frac{1/2}{a\cos\varphi_{j+1/2} \Delta\lambda} \\ zfpvoy(j) &= \frac{1/2}{a\cos\varphi_{j+1/2} \Delta\varphi} \end{aligned}$$

2. vertical advection of u:

$$\begin{aligned} zfkpx_{i+1/2,j,k+1/2} &= \frac{1}{2}\frac{w^*_{i,j,k+1/2} + w^*_{i+1,j,k+1/2}}{\Delta\left(p_0\right)_k + \Delta\left(p_0\right)_{k+1}} \\ zfkmx_{i+1/2,j,k-1/2} &= \frac{1}{2}\frac{w^*_{i,j,k-1/2} + w^*_{i+1,j,k-1/2}}{\Delta\left(p_0\right)_k + \Delta\left(p_0\right)_{k-1}} \end{aligned}$$

3. vertical advection of v:

$$\begin{aligned} zfkpx_{i,j+1/2,k+1/2} &= \frac{1}{2}\frac{w^*_{i,j,k+1/2} + w^*_{i,j+1,k+1/2}}{\Delta\left(p_0\right)_k + \Delta\left(p_0\right)_{k+1}} \\ zfkmx_{i,j+1/2,k-1/2} &= \frac{1}{2}\frac{w^*_{i,j,k-1/2} + w^*_{i,j+1,k-1/2}}{\Delta\left(p_0\right)_k + \Delta\left(p_0\right)_{k-1}} \end{aligned}$$

4. vertical advection of w:

$$\begin{aligned} zgcvx_{i,j,k} &= \frac{1}{4}\frac{w^*_{i,j,k-1/2} + w^*_{i,j,k+1/2}}{\Delta\left(p_0\right)_k} \\ zgavx_{i,j,k-1} &= \frac{1}{4}\frac{w^*_{i,j,k-11/2} + w^*_{i,j,k-1/2}}{\Delta\left(p_0\right)_{k-1}} \end{aligned}$$

In none of the previous equations a flux limiter does occur. The equations are not written in flux form.

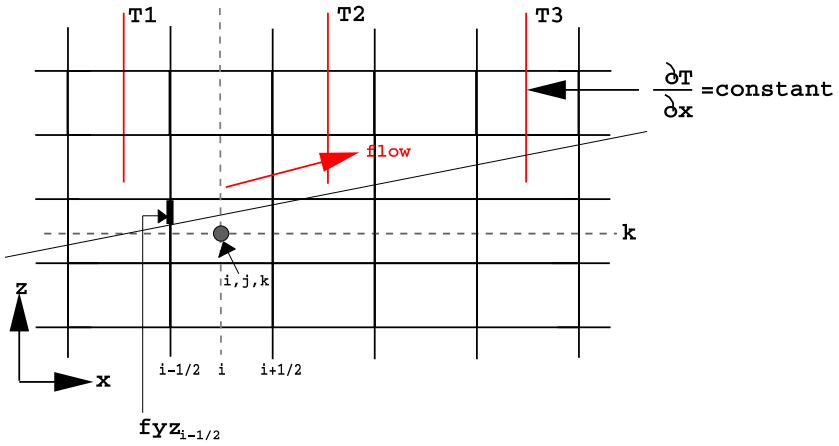

FIGURE 2.11a: Definition of the flux limiter in the grid.

Fig. 2.11a and Fig. 2.11b illustrate why the introduction of flux limiters in the advection terms would be faulty. The flux limiter $fyz_{i-1/2}$ is the fraction of the free interface of the volume $_{i,j,k}$ divided by the total area $\Delta y \Delta z$ of the interface. The so defined flux limiters take values between 0 and 1. If for example the temperature gradient $\frac{\partial T}{\partial x}$ is constant and the flow vector is parallel to the mountain's slope and constant with height, that means, a uniform flow uphill, then the advection $-u\frac{\partial T}{\partial x}$ is constant in the entire domain shown in Fig. 2.11a. Thus the volume element at $_{i,j,k}$ which is cut by mountains slope experiences the same temperature advection as all the other volume elements. For the mentioned volume element:

$$\frac{\partial T}{\partial t} = \underline{-fyz_{i-1/2}} u_{i-1/2} \left.\frac{\partial T}{\partial x}\right|_{i-1/2} \qquad \text{wrong!!} \qquad (50)$$

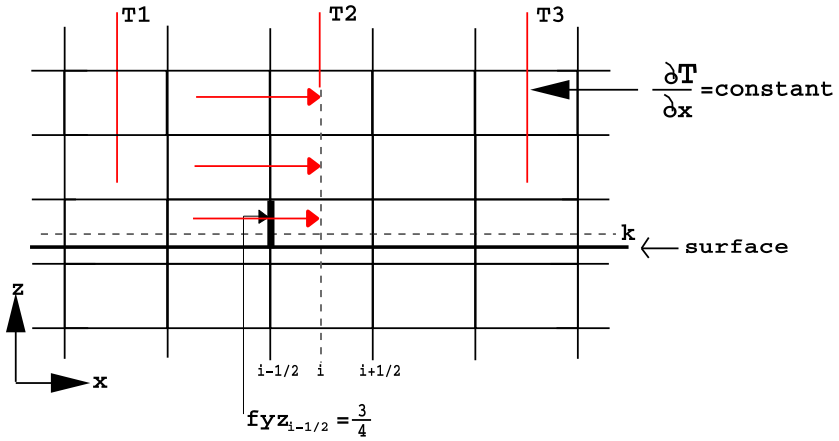

FIGURE 2.11b: Flux limiters for $\frac{\partial T}{\partial x}$ in the case of a horizontal terrain.

Fig. 2.11b illustrates the same situation in a simpler case. The current is uniform in x-direction and $\frac{\partial T}{\partial x} = const.$ The temperature gradient is assumed to be constant $\frac{\partial}{\partial z}\left(\frac{\partial T}{\partial x}\right) = 0$. The temperature tendency due to the advection $\frac{\partial T}{\partial t} = -u\frac{\partial T}{\partial x}$ is constant in the entire domain. If the surface would fill $\frac{1}{4}$ of the volume elements at level k, the free interfaces fyz of all the volume elements at that level would be $\frac{3}{4}$. If the carrier velocity u were premultiplied

by $fyz = \frac{3}{4}$ at level k, this would reduce the temperature tendency due to the advection of 25%, which would be wrong!

The explained treatment of the boundary values has to be done with much carefulness. The calculation of the corrrect derivatives close to the boundary are most important. The respond of the flow field is very sensitive with respect to the calculation of the boundary.

3 Time Integration and Numerical Solution

3.1 Fast Tendencies

According to the mode splitting time integration method proposed by Klemp and Wilhelmson (1978) the time step for stable explicit integration of the slow modes is subdivided into a number of small time steps. The tendencies represented in equations (1.21) - (1.25) are computed only once every big time step.

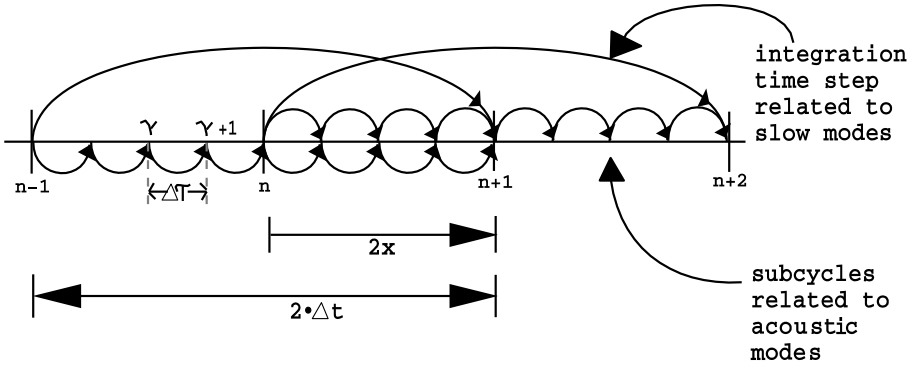

FIGURE 3.1: The Klemp Wilhelmson scheme.

Fig. 3.1 visualizes the mode splitting technique. The sound waves show up in the pressure gradient force, in the horizontal and vertical wind velocity and in the divergence term of the pressure tendency equation. High frequency oscillation is also caused by the buoyancy term. Additionally the vertical gravity wave propagation is also included in the reduced set of equations (1.21) - (1.25). As one can see from Fig. 3.1 the time step from n to $n+1$ is computet two times in the subcycle procedure. This will later be one of the reasons for approaches of a two time level integration scheme. The reduced set of equations which becomes subject to a split time integration using small time steps is revealed by rewriting the model equations (1.10) - (1.14) for the wind components, the pressure perturbation and the temperature in the following form:

$$\frac{\partial u}{\partial t} = \frac{1}{\rho a \cos^{\varphi}} \frac{\partial p'}{\partial \lambda} + f_u \tag{51}$$

$$\frac{\partial v}{\partial t} = \frac{1}{\rho a} \frac{\partial p'}{\partial \varphi} + fv \tag{52}$$

$$\frac{\partial w}{\partial t} = \frac{g}{\Delta p_0} \frac{\rho_0}{\rho} \frac{\partial p'}{\partial \zeta} + g \frac{\rho_0}{\rho} \left[\frac{T - T_0}{T} - \frac{T_0}{T} \frac{p'}{p_0} \right] + f_w \tag{53}$$

$$\frac{\partial p'}{\partial t} = g\rho_0 w - \frac{c_p}{c_v} p \left[D_h - \frac{g\rho_0}{\Delta p_0} \frac{\partial w}{\partial \zeta} \right] + f_{p'} \tag{54}$$

$$\frac{\partial T}{\partial t} = \frac{1}{\rho c_v} p \left[D_h - \frac{g\rho_0}{\Delta p_0} \frac{\partial w}{\partial \zeta} \right] + f_T \tag{55}$$

The threedimensional divergence D_3 in equation (1.7) is separated into a horizontal part D_h

$$D_h = \frac{1}{a\cos\varphi}\left[\frac{\partial u}{\partial \lambda} + \frac{\partial}{\partial \varphi}\left(v\cos\varphi\right)\right] \tag{56}$$

and a vertical part D_v

$$D_v = -\frac{g\rho_0}{\Delta p_0}\frac{\partial w}{\partial \zeta} \tag{57}$$

where the transformation (1.26) was applied in order to rewrite $\frac{\partial}{\partial z}$.

The set of equation (2.1) - (2.5) with acoustically active terms the big leapfrog time step $2\Delta t$ (see fig. 2.1) is subdivided into a number of small timesteps $\Delta\tau$. $2\Delta t$ must be an integer number times the small time step $\Delta\tau$. $\Delta\tau$ is determined by the fastest signal velocity, this means the sound speed:

$$\Delta\tau \leq \frac{\Delta s}{\sqrt{2}c_s} \qquad c_s = \text{ velocity of sound} \tag{58}$$

Δs is the horizontal spatial gridsize, $\Delta s = a\Delta\lambda = a\Delta\varphi$ with $\cos\varphi = 1$, supposed $\Delta\lambda = \Delta\varphi$. The vertical gridsize does not matter as long as the integration is carried out implicitely. For test cases the integration is sometimes carried out explicitely, then $\Delta\tau$ is limited by

$$\Delta\tau \leq \frac{\Delta z_{min}}{\sqrt{2}c_s} \tag{59}$$

where Δz_{min} is the minimum vertical grid spacing (usually this is the thickness of the lowest model layer).

Concerning the finite difference algorithms related to fast modes, second-order accurate differencing is used for spatial discretization of the reduced set of equations (2.1) - (2.5). The vertical velocity, the pressure pertubation and in the current model also $T - T_0$ are subject to time averaging with respect to the small time step $\Delta\tau$. Time averaging is realized in the same way as in the program code of the operationel LM

$$\overline{\psi}^{\tau} = \frac{1}{2}\left(1+\beta_{sw}\right)\psi^{\nu+1} + \frac{1}{2}\left(1-\beta_{sw}\right)\psi^{\nu}$$

see LM operational version (Doms and Schaettler, 1999). $\nu + 1$ is the future time level related to the small steps $\Delta\tau$. The subcycle procedure is a 2 time level integration scheme. To simplify the notations we write

$$\beta^{+} = \frac{1}{2}\left(1+\beta_{sw}\right) \qquad \text{and} \qquad \beta^{-} = \frac{1}{2}\left(1-\beta_{sw}\right) = 1-\beta^{+}$$

the model uses $\beta_{sw} = 0.4$ (i.e. $\beta^{+} = 0.7$, $\beta^{-} = 0.3$). The time averaging is then realized with

$$\overline{\psi}^{\tau} = \beta^{+}\psi^{\nu+1} + \beta^{-}\psi^{\nu} \qquad \text{for} \qquad \psi = w, p', (T-T_0) \tag{60}$$

The finite difference equations derived from (2.1) - (2.6) are written in the following form, using definitions from Section 2.4.

$$u^{\nu+1} - u^{\nu} = -\frac{\Delta\tau}{\overline{\rho^n}^{\lambda} a\overline{\cos^{\varphi}\varphi}^{\varphi}\Delta\lambda}\delta_{\lambda}p'^{\nu} + f_u^n\Delta\tau \tag{61}$$

$$v^{\nu+1} - v^{\nu} = -\frac{\Delta\tau}{\overline{\rho^n}^{\varphi} a\Delta\varphi}\delta_{\varphi}p'^{\nu} + f_v^n\Delta\tau \tag{62}$$

$$\begin{aligned} w^{\nu+1} - w^{\nu} = {} & g\frac{\Delta\tau}{\Delta p_o}\frac{\overline{\rho_0}^{h\zeta}}{\overline{\rho^n}^{h\zeta}}\left[\beta^+\delta_{\zeta}\left(p'\right)^{\nu+1} + \beta^-\delta_{\zeta}\left(p'\right)^{\nu}\right] \\ & -g\Delta\tau\frac{\overline{\rho_0}^{h\zeta}}{\overline{\rho^n}^{h\zeta}}\left[\beta^+\overline{\frac{T_0}{T^n p_0}p'^{\nu+1}}^{h\zeta} + \beta^-\overline{\frac{T_0}{T^n p_0}p'^{\nu}}^{h\zeta}\right] \\ & -g\Delta\tau\frac{\overline{\rho_0}^{h\zeta}}{\overline{\rho^n}^{h\zeta}}\left[\beta^+\overline{\frac{T^{\nu+1}-T_0}{T^n}}^{h\zeta} + \beta^-\overline{\frac{T^{\nu}-T_0}{T^n}}^{h\zeta}\right] + f_w^n\Delta\tau \end{aligned} \tag{63}$$

$$\begin{aligned} p'^{\nu+1} - p'^{\nu} = {} & g\rho_0\Delta\tau\left[\beta^+\overline{w^{\nu+1}}^{m\zeta} + \beta^-\overline{w^{\nu}}^{m\zeta}\right] \\ & +g\frac{\rho_0\Delta\tau}{\Delta p_0}\frac{p^n c_p}{c_v}\left[\beta^+\delta_{\zeta}\left(fxyw^{\nu+1}\right) + \beta^-\delta_{\zeta}\left(fxyw^{\nu}\right)\right] \\ & -\Delta\tau\frac{p^n c_p}{c_v}D_h^{\nu+1} + f_{p'}^n\Delta\tau \end{aligned} \tag{64}$$

$$\begin{aligned} T^{\nu+1} - T^{\nu} = {} & g\frac{\rho_0\Delta\tau}{\Delta p_0}\frac{p^n}{\rho^n c_v}\left[\beta^+\delta_{\zeta}\left(fxyw^{\nu+1}\right) + \beta^-\delta_{\zeta}\left(fxyw^{\nu}\right)\right] \\ & -\Delta\tau\frac{p^n}{\rho^n c_v}D_h^{\nu+1} + f_T^n\Delta\tau \end{aligned} \tag{65}$$

The horizontal divergence D_h is computed at the centre of a grid box i, j, k even then when the volume contains only a little piece of air. The horizontal divergence reads:

$$D_h^{\nu+1} = \frac{1}{a\overline{\cos\varphi^{\varphi}}\Delta\lambda}\delta_{\lambda}\left(fyzu^{\nu+1}\right) + \frac{1}{a\overline{\cos\varphi}^{\varphi}\Delta\varphi}\delta_{\varphi}\left(\cos\varphi fxzv^{\nu+1}\right) \tag{66}$$

the vertical part D_v of equation (2.7) is:

$$D_v = \beta^+\delta_{\zeta}\left(fxyw^{\nu+1}\right) + \beta^-\delta_{\zeta}\left(fxyw^{\nu}\right) \tag{67}$$

The horizontal divergence D_h is first computed with the new velocities $u^{\nu+1}$ and $v^{\nu+1}$ at the new time level $\nu+1$. The equations (2.11), (2.12) and (2.16) remain in the explicit part of the integration procedure if the calculation is carried out implicitely. Most important now is the occurence of the so called flux limiters fxz, fyz and fxy. The last two letters denote the interfaces of a control volume, see Fig. 2.2. xz for example denotes an interface stretched in the xz-plane. All the flux limiters are non dimensional numbers between 0 and 1.

$fxy = \frac{s_{xy}}{\Delta x\Delta y}$ where s_{xy} is the real free interface expressed in m^2 and $\Delta x\Delta y$ is the total area of the interface. In case of fyz that reads: $fyz = \frac{s_{yz}}{\Delta y\Delta z}$. Only through these factors, in the divergence term the current feel the boundary. If the slope is small, $\frac{\Delta z}{\Delta x} < 1$ the factors are decreasing smoothly to zero as the flow is running in x-direction. Thus the current does not notice a step size topography but a smooth terrain as it should be. This is the most important difference of the shaved element method with respect to the Legoland topography. In equation (2.14) the flux limiters are affecting the pressure and the pressure again affects the vertical velocity. The term $g\rho_0 w$ is not premultiplied by the flux limiters. As we see, the

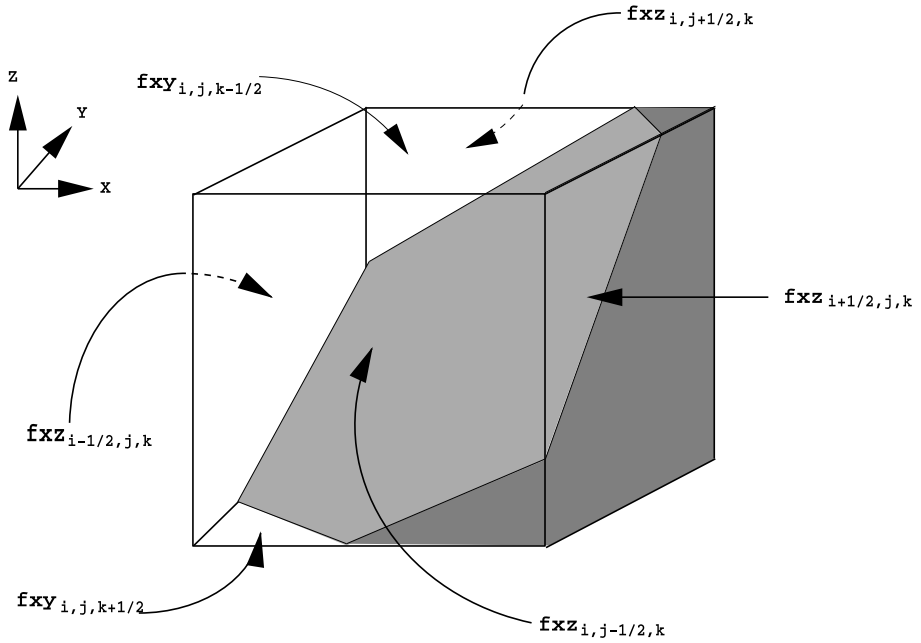

FIGURE 2.2: Flux limiters in three dimensions.

reference atmosphere is hiding here.

$$\begin{aligned} \frac{\partial p_0}{\partial z} &= -g\rho_0 \qquad \text{this implies} \\ g\rho_0 w &= -w\frac{\partial p_0}{\partial z} \end{aligned}$$

but $-w\frac{\partial p_0}{\partial z}$ is an advection term and above it was stated that the advection must be without a flux limiter.

3.2 Method of Solution

A vertically implicit integration scheme is applied for the solution of equation (2.1) - (2.5). Equations (2.3), (2,4) and (2.5) for the vertical velocity, the pressure perturbation and the temperature become coupled due to time averaging. In the current version the temperature deviation term

$$\frac{T^\nu - T_0}{T^n}$$

is drawn into the implicit calculation procedure. The temperature equation (2.15) in differencing form can be written as follows:

$$T_k^{\nu+1} = T_k^\nu + R_k \tag{68}$$

where R_k is the rest of the right hand side of equation. From (2.18) we gain:

$$T_k^{\nu+1} - (T_0)_k = T_k^\nu - (T_0)_k + R_k$$

respectively

$$\frac{T_k^{\nu+1} - (T_0)_k}{T_k^n} = \frac{T_k^\nu - (T_0)_k}{T_k^n} + \frac{R_k}{T_k^n} \tag{69}$$

In (2.19) we call $\frac{T_k^{\nu+1}-(T_0)_k}{T_k^n} = s_k^{\nu+1}$ and

$$\frac{T_k^\nu - (T_0)_k}{T^n} = s_k^\nu \qquad \text{(2.19) then becomes}$$

$$s_k^{\nu+1} = s_k^\nu + \frac{R_k}{T_k^n} \tag{70}$$

with the substitutions (A.1) - (A.7), see appendix, the equation for the vertical velocity (2.13) can be written in the following way:

$$\begin{aligned} w_{k-1/2}^{\nu+1} - w_{k-1/2}^\nu = {} & g\Delta\tau 2y_{k-1/2}\left[\beta^+\left(p_k^{\nu+1} - p_{k-1}^{\nu+1}\right) + \beta^-\left(p_k^\nu - p_{k-1}^\nu\right)\right] \\ & -g\Delta\tau\beta^+ 2y_{k-1/2}\left[(\Delta p_0)_{k-1}\frac{1}{2}x_k p_k^{\nu+1} + (\Delta p_0)_k\frac{1}{2}x_{k-1}p_{k-1}^{\nu+1}\right] \\ & -g\Delta\tau\beta^- 2y_{k-1/2}\left[(\Delta p_0)_{k-1}\frac{1}{2}x_k p_k^{\nu} + (\Delta p_0)_k\frac{1}{2}x_{k-1}p_{k-1}^{\nu}\right] \\ & +g\Delta\tau\beta^+ 2y_{k-1/2}\left[(\Delta p_0)_{k-1}\frac{1}{2}s_k^{\nu+1} + (\Delta p_0)_k\frac{1}{2}s_{k-1}^{\nu+1}\right] \\ & +g\Delta\tau\beta^- 2y_{k-1/2}\left[(\Delta p_0)_{k-1}\frac{1}{2}s_k^{\nu} + (\Delta p_0)_k\frac{1}{2}s_{k-1}^{\nu}\right] \end{aligned} \tag{71}$$

After reorganizing the terms and applying (A.8) - (a.10), see appendix, the equation for the vertical velocity reads:

$$\begin{aligned} w_{k-1/2}^{\nu+1} = {} & w_{k-1/2}^\nu + C_{k-1/2}^w + \beta^+ C_{k-1/2}^{w1}\left[\alpha_{k-1/2}^B p_k^{\nu+1} - \alpha_{k-1/2}^T p_{k-1}^{\nu+1}\right. \\ & \left. + \left((\Delta p_0)_{k-1}\frac{1}{2}s_k^{\nu+1} + (\Delta p_0)_k\frac{1}{2}s_{k-1}^{\nu+1}\right)\right] \end{aligned} \tag{72}$$

$$\begin{aligned} C_{k-1/2}^w = {} & \left(f_w^n\right)_{k-1/2}\Delta\tau + \beta^- C_{k-1/2}^{w1}\left[\alpha_{k-1/2}^B p_k^{\nu} - \alpha_{k-1/2}^T p_{k-1}^{\nu}\right. \\ & \left. + \left((\Delta p_0)_{k-1}\frac{1}{2}s_k^{\nu} + (\Delta p_0)_k\frac{1}{2}s_{k-1}^{\nu}\right)\right] \end{aligned} \tag{73}$$

consequently the pressure tendency equation from (2.14) reads in differencing form:

$$\begin{aligned} p_k^{\nu+1} - p_k^\nu = {} & \left(f_p^n\right)_k\Delta\tau - \frac{p_k^n c_p}{c_v}\left(D_h^{\nu+1}\right)_k\Delta\tau + \beta^-\frac{1}{2}g\Delta\tau\left(\rho_0\right)_k \\ & \left(w_{k+1/2}^\nu + w_{k-1/2}^\nu\right) + \beta^-\frac{g\left(\rho_0\right)_k}{(\Delta p_0)_k}\frac{p_k^n c_p}{c_v}\Delta\tau \\ & \left(fxy_{k+1/2}w_{k+1/2}^\nu - fxy_{k-1/2}w_{k-1/2}^\nu\right) + \beta^+\frac{1}{2}g\Delta\tau \\ & \left(\rho_0\right)_k\left(w_{k+1/2}^{\nu+1} + w_{k-1/2}^{\nu+1}\right) + \beta^+\frac{g\left(\rho_0\right)_k}{(\Delta p_0)_k}\frac{p_k^n c_p}{c_v}\Delta\tau \\ & \left(fxy_{k+1/2}w_{k+1/2}^{\nu+1} - fxy_{k-1/2}w_{k-1/2}^{\nu+1}\right) \end{aligned} \tag{74}$$

Applying (A.11) and (A.12), (2.24) reads:

$$p_k^{\nu+1} = p_k^\nu + C_k^p + \beta^+ C_k^{p2}\left(w_{k+1/2}^\nu + w_{k-1/2}^\nu\right) + \beta^+ C_k^{p1} \left(fxy_{k+1/2} w_{k+1/2}^{\nu+1} - fxy_{k-1/2} w_{k-1/2}^{\nu+1}\right) \tag{75}$$

$$C_k^p = \left(f_p^n\right)_k \Delta\tau - \frac{p_k^n c_p}{c_v}\Delta\tau \left(D_h^{\nu+1}\right)_k + \beta^- C_k^{p2} \left(w_{k+1/2}^\nu + w_{k-1/2}^\nu\right) + \beta^- C_k^{p1}\left(fxy_{k+1/2} w_{k+1/2}^\nu - fxy_{k-1/2} w_{k-1/2}^\nu\right) \tag{76}$$

The temperature equation (2.15) completes the set of differencing equations:

$$T_k^{\nu+1} = T_k^\nu + \left(f_T^n\right)_k \Delta\tau - \frac{p_k^n}{\rho_k^n c_v}\Delta\tau \left(D_h^{\nu+1}\right)_k + \frac{g\left(\rho_0\right)_k \Delta\tau}{\left(\Delta\rho_0\right)_k}\frac{p_k^n}{\rho_k^n c_v}\left[\beta^+\left(fxy_{k+1/2} w_{k+1/2}^{\nu+1} - fxy_{k-1/2} w_{k-1/2}^{\nu+1}\right) + \beta^-\left(fxy_{k+1/2} w_{k+1/2}^\nu - fxy_{k-1/2} w_{k-1/2}^{\nu+1}\right)\right] \tag{77}$$

As can be seen, the flux limiters show up in the vertical derivative of w, which is the vertical part of the divergence and they occur also in the horizontal part of the divergence $D_h^{\nu+1}$. For the vertically implicit solution procedure equations (2.22), (2.25) and (2.27) form a coupled system. Eliminating $p_k^{\nu+1}$ and $s_k^{\nu+1}$ at the future time step the w-equation (2.22) leaves $w^{\nu+1}$ as the only unknown. In order to eliminate $p_k^{\nu+1}$ and $p_{k-1}^{\nu+1}$ we use equation (2.25). The derivation of the additional term in (2.22)

$$\left(\left(\Delta p_o\right)_{k-1}\frac{1}{2}s_k^{\nu+1} + \left(\Delta p_0\right)_k \frac{1}{2}s_{k-1}^{\nu+1}\right) \tag{78}$$

which contains the vertical velocities at time step $\nu+1$ too is outlined in the appendix (A.13) - (A.16). Finally (A.15) with (A.16) are used in order to substitute the parenthesis (2.28) in the equation for the vertical velocity (2.22). After rearranging the terms this yields a linear tridiagonal equation system for $w^{\nu+1}$ which is written in the form:

$$a_{k-1/2} w_{k-11/2}^{\nu+1} + b_{k-1/2} w_{k-1/2}^{\nu+1} + c_{k-1/2} w_{k+1/2}^{\nu+1} = d_{k-1/2} \tag{79}$$

The matrix diagonals a, b and c and the inhomogeneous part d read:

$$a_{k-1/2} = -\beta^{+2} C_{k-1/2}^{w1}\left[\alpha_{k-1/2}^T\left(C_{k-1}^{p1} fxy_{k-11/2} - C_{k-1}^{p2}\right) - \left(\Delta p_0\right)_k C_{k-1}^{T1} fxy_{k-11/2}\right] \tag{80}$$

$$b_{k-1/2} = 1 + \beta^{+2} C_{k-1/2}^{w1}\left[\alpha_{k-1/2}^B\left(C_k^{p1} fxy_{k-1/2} - C_k^{p2}\right) + \alpha_{k-1/2}^T \left(C_{k-1}^{p1} fxy_{k-1/2} + C_{k-1}^{p2}\right) + \left(\Delta p_0\right)_{k-1} C_k^{T1} fxy_{k-1/2} - \left(\Delta p_0\right)_k C_{k-1}^{T1} fxy_{k-1/2}\right] \tag{81}$$

$$c_{k-1/2} = -\beta^{+2} C_{k-1/2}^{w1}\left[\alpha_{k-1/2}^B\left(C_k^{p1} fxy_{k+1/2} + C_k^{p2}\right) + \left(\Delta p_0\right)_{k-1} C_k^{T1} fxy_{k+1/2}\right] \tag{82}$$

$$d_{k-1/2} = w_{k-1/2}^\nu + C_{k-1/2}^w + \beta^+ C_{k-1/2}^{w1}\left[\alpha_{k-1/2}^B\left(p_k^\nu + C_k^p\right) - \alpha_{k-1/2}^T \left(p_{k-1}^\nu + C_{k-1}^p\right) + C_{k-1/2}^T\right] \tag{83}$$

The coefficients contain the flux limiters fxy and some additional terms with factors C^{T1} and C^T in the inhomogeneous part d which have their origin in the temperature equation. Actually, according to a suggestion of Janjic (19xx), the vertical advection of pressure pertubation $w\frac{\partial p'}{\partial z}$ should also be put into the implicit scheme - this wopuld further stabilize the integration. The matrix equation (2.29) can be solved for $w^{\nu+1}$ using a standard tridiagonal solver, provided that the vertical velocity at the upper and lower boundary is specified. At the top boundary the vertical velocity is set to zero. At the lower boundary we must allow the flow running parallel to the slope. Thus an appropriate value for w has to be taken at the lower boundary.

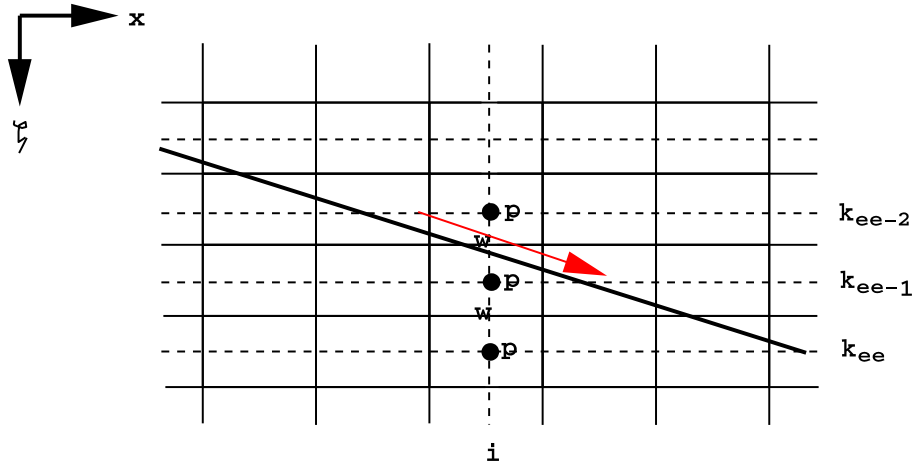

FIGURE 2.3: Boundary values of w under the surface

In Fig. 2.3 the volume element at $_{i,kee}$ lies completely under the surface. The prognostic equation (2.21) for the vertical velocity at $_{i,kee-11/2}$ requires the two pressure values $p_{i,kee-1}$ and $p_{i,kee-2}$ in order to calculate the pressure gradient at $_{i,kee-11/2}$. Since the pressure at $_{i,kee-1}$ is available this is no problem. The pressure at $_{i,kee-1}$ needs the vertical velocity at $_{i,kee-1/2}$. Normally this velocity would be not available but because it is a boundary value which is calculated according to equation (1.39) or (1.42) respectively. In the current model (1.39) or (1.42) is applied every small time step $\Delta\tau$. This is better rather than holding the boundary values constant during the entire subcycle procedure. The best value for the vertical velocity would yield if $w_{i,kee-1/2}$ were calculated dependent on the horizontal velocity with the demand that the total flow vector $\vec{v} = (u, v, w)$ at the surface is exactly tangential to the surface. Such a method is not implemented yet.

3.1 Structure of the Tridiagonal Matrix

In Section 1 the boundary values, necessary for the calculation of the derivatives close to the boundary were explained. The implicit scheme is related to the elimination of $w^{\nu+1}$ in a vertical column. The vertical do loop starts at k+1/2 and would normally end at $_{kee-1/2}$ because $w_{kee-1/2}$ is the lower boundary value. But kee is dependent on the orography, that means, kee is a function of i and j: kee = f(i,j) or in the current model: kee = kfin(i,j). The field kfin(i,j), contains the lowest k values at i,j this is the lowest level for w, the location of the lower boundary value. kfin(i,j) is calculated at the beginning of the program run in subroutine src_artifdata.f90 or z_level.f90 and is available in fast_waves.f90. The end of the do loop in vertical direction would be kee which is a function of i,j. Thus the k-loop had to be disposed to the interior of loop i and j; but this is not suitable. The tridiagonal equation system for $w^{\nu+1}$ runs as follows see Fig. 3.4.

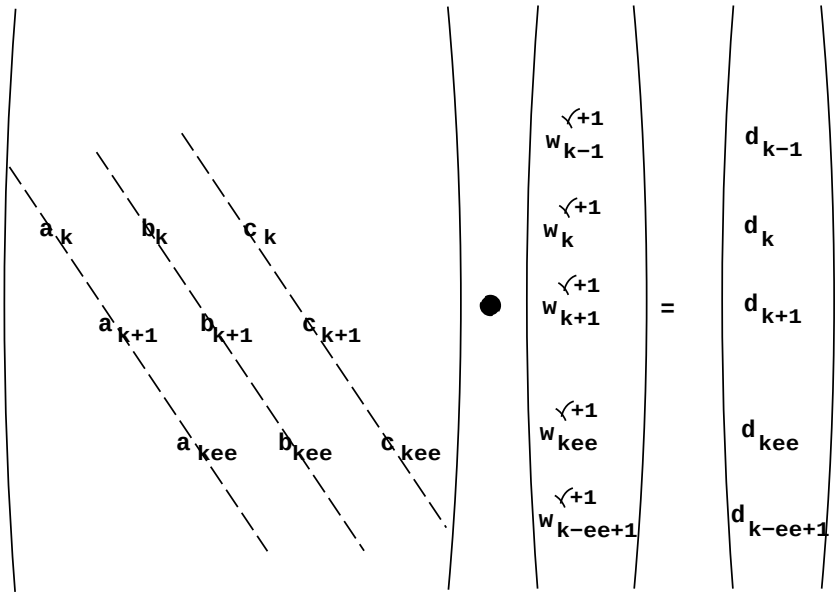

FIGURE 3.4: The matrix of the 1-d implicit scheme.

If we demand from the matrix system that the boundary value w_{kee} should be retrieved, then the coefficients and the inhomogeneous part read:

$$\begin{aligned} a_{kee} &= 0 \\ b_{kee} &= 1 \\ c_{kee} &= 0 \\ d_{kee} &= w^{\nu}_{kee} \end{aligned}$$

With these values w^{ν}_{kee} is reproduced in $w^{\nu+1}_{kee}$

For k > kee we set:

$$\begin{aligned} a_k &= 0 \\ b_k &= 1 \\ c_k &= 0 \\ d_k &= 0 \end{aligned}$$

which generates $w^{\nu+1}_k = 0$ for k > kee.

With this structure of tridiagonal system the do loops within the Gauss solver can be nested in the normal way: k-loop outside, j- and i-loop inside, and again this constellation is supposed to be numerically efficient.

4 Numerical Smoothing

4.1 Horizontal Diffusion

The program needs horizontal and vertical diffusion. At some boundaries some action is necessary in order to process the derivatives close to the boundaries. Here the second order

differencing scheme breaks down to order one. But there is another serious problem. Since the model only uses the complete spatial differences in the derivatives this implies very high errors for small volume elements in the calculation of the divergence term which acts on the pressure tendency equation (see Fig. 4.1). If the volume element is very small it kills the program run immedeately before one big time step is completed.

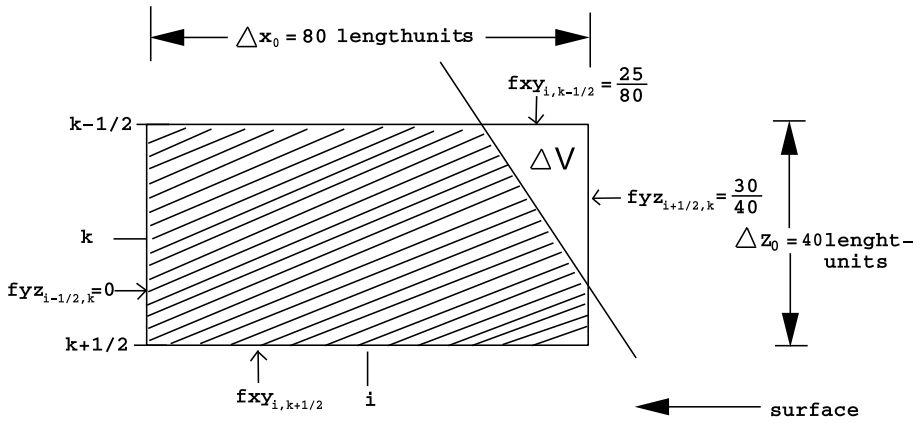

FIGURE 4.1: A small cut cell

Fig. 4.1 illustrates why this error occurs in the divergence term or in the pressure tendency equation which is used to represent the continuity equation. The correct volume Δv can be calculated as:

$$\Delta V = \frac{1}{2} fxy_{i,k-1/2} fxy_{j+1/2,k} \Delta x_0 \Delta z_0 \tag{84}$$

$$\begin{aligned} \frac{\Delta M}{\Delta t} = & -\rho(\Delta v)\left[\left(fyz_{i+1/2,k}u_{i+1/2,k} - fyz_{i-1/2,k}u_{i-1/2,k}\right)\Delta z_0\right. \\ & \left. + \left(fxy_{i,k-1/2}w_{i,k-1/2} - fxy_{i,k+1/2}w_{i,k+1/2}\right)\Delta x_0\right] \end{aligned} \tag{85}$$

Equation (3.1) represents the change of mass within the triangle ΔV. The continuity equation is retrieved by dividing (3.1) by ΔV :

$$\begin{aligned} \frac{\frac{\Delta M}{\Delta V}}{\Delta t} = & -\rho(\Delta v)\left[\left(fyz_{i+1/2,k}u_{i+1/2,k} - fyz_{i-1/2,k}u_{i-1/2,k}\right)\right. \\ & \frac{\boldsymbol{\Delta z_0}}{\frac{1}{2}fxy_{i,k-1/2}fyz_{i+1/2,k}\Delta x_0 \boldsymbol{\Delta z_0}} + \left(fxy_{i,k-1/2}w_{i,k-1/2}\right. \\ & \left.\left. - fxy_{i,k+1/2}w_{i,k+1/2}\right)\frac{\boldsymbol{\Delta x_0}}{\frac{1}{2}fxy_{i,k-1/2}fyz_{i+1/2,k}\boldsymbol{\Delta x_0}\Delta z_0}\right] \end{aligned} \tag{86}$$

divided by $\rho(\Delta v)$ yields:

$$\begin{aligned} \frac{1}{\rho}\frac{\Delta \rho}{\Delta t} = & -\left[\frac{1}{\Delta x_0}\left(fyz_{i+1/2,k}u_{i+1/2,k} - fyz_{i-1/2,k}u_{i-1/2,k}\right)\right. \\ & \frac{1}{\frac{1}{2}fxy_{i,k-1/2}fyz_{i+1/2,k}} + \frac{1}{\Delta z_0} \\ & \left(fxy_{i,k-1/2}w_{i,k-1/2} - fxy_{i,k+1/2}w_{i,k+1/2}\right) \\ & \left.\frac{1}{\frac{1}{2}fxy_{i,k-1/2}fyz_{i+1/2,k}}\right] \end{aligned} \tag{87}$$

From equation (3.4) it becomes obvious why the continuity equation or in the current model the pressure tendency equation cannot work for small volume elements. The current model uses the complete differences $\frac{1}{\Delta x_0}$ and $\frac{1}{\Delta z_0}$ but in reality the volume element is much smaller, the space differences Δx_0 and Δz_0 have to be premultiplied by $\left(\frac{1}{2} fxy_{i,k-1/2} fyz_{i+1/2,k}\right)$. This factor is missing in the current model. Unfortunately this factor can be of any smallness and in addition the factor would occure in the horizontal part of the divergence too. This is outside the implicit computation procedure which is directed only in the vertical. Thus the stability criterion would be dependent on the smallest volume element if the factor would be taken into account.

In order to overcome the problem we have to remove the very small volume elements. This is done in subroutine src_artifdata.f90 or in z_level.f90 respectively. Generally volume elements smaller than 1/60 or 1/120 of the total volume of an element are removed. In idealized experiments with a smooth Gaussian mountain the surface will be much rougher. The other volume elements greater than 1/60 or 1/120 are still not calculated correctly because of the mentioned missing factor in the divergence term. The current model is suffering from these deficiencies. The incorrect calculation of the derivatives in the divergence term results into wrong tendencies which appear as an overreaction and creates peaks of the parameters when stepped forward. Of course those peaks show up in the cut volume elements this means direct at the boundary. When we apply a diffusion in order to damp down the overreaction it should mainly act direct at the boundary. The horizontal diffusion is carried out sequentially, first in x- then in y-direction. The fourth order diffusion is drawn to the boundary in the following way:

```
work = 0
!
  do j = jstart-1 , jend+1
  do i = istart-1 , iend+1
    work(i,j) = weight(i+1,j)*(s(i+1,j)-s(i,j)) &
              - weight(i-1,j)*(s(i,j)-s(i-1,j))
  enddo
  enddo
!
  do j = jstart-1 , jend+1
  do i = istart-1 , iend+1
    dcoeff1 = dcoeff
    if((weight(i+1,j) < 0.5).and.(weight(i,j) > 0.5) dcoeff1 = alam
    if((weight(i-1,j) < 0.5).and.(weight(i,j) > 0.5) dcoeff1 = alam
    zsten = -dcoeff1*(weight(i+1,j)-(work(i+1,j)-work(i,j)) &
                     -weight(i-1,j)-(work(i,j)-work(i-1,j)))
!
    sten(i,j) = sten(i,j)+zsten
  enddo
  enddo
endif
```

In case if there is no boundary, the weight-factors are all 1. In this case the diffusion is working like in the operational LM with dcoeff1 = dcoeff which is the diffusion coefficient of the operational version. Now if the boundary is at the east side (see Fig. 4.2) the value at i+1 is beyond the boundary and weight (i+1,j) = 0. The program code above is acting in the following way:

$$\begin{aligned} work\,(i,j) &= -\Delta s_1 & \Delta s_1 &= s\,(i,j) - s\,(i-1,j) \\ work\,(i-1,j) &= \Delta s_1 - \Delta s_2 & \Delta s_2 &= s\,(i-1,j) - s\,(i-2,j) \end{aligned}$$

$$\begin{aligned} zsten &= -alam\,[-\,(work\,(i,j) - work\,(i-1,j))] \\ zsten &= alam\,[work\,(i,j) - work\,(i-1,j)] \\ zsten &= alam\,[\Delta s_2 - 2\Delta s_1] \end{aligned} \tag{88}$$

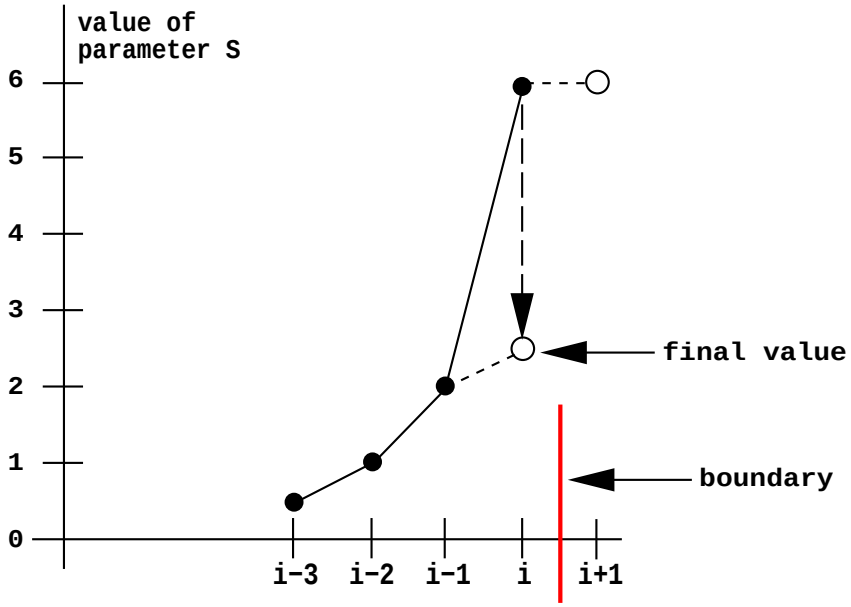

FIGURE 4.2: Action of horizontal diffusion

In the example of Fig. 4.2 $\Delta s_1 = 4$ and $\Delta s_2 = 1$ the tendency according to diffusion yields:

$$zsten = -7alam \tag{89}$$

zsten is negativ which implies, the fluctuating crazy boundary value s(i,j) = 6 is towed to lower values and calmed down. The final value, indicated in Fig. 4.2 with the short dashed line will be 2.5. Then $\Delta s_1 = \frac{1}{2}\Delta s_2$ and according to equation (3.5) zsten = 0. If a boundary is there the diffusion coefficient changes to

$$alam = \frac{1}{12dt2} \tag{90}$$

As illustrated in Fig. 4.2 the final value, caused by the diffusion, fits well into the general spatial distribution of the parameter s. But still the final value cannot represent the exact gradient of s if the gradient is unequal zero. Only if $\frac{\partial s}{\partial x} = 0$ then $\Delta s_2 = 0$ and from $\Delta s_1 = \frac{1}{2}\Delta s_2$ follows $\Delta s_1 = 0$; this implies, the final value s_i would be on the straight line defined by s_{i-2} and s_{i-1}. But it is very important to represent the correct vertical gradients of the velocity components and the temperature. The diffusion must not bend the profile off the gradient which has been established at gridpoints above the obstacle.

4.1 Vertical Diffusion

In order to sustain the established vertical gradient of the velocity and the temperature, the vertical diffusion in the current model effects on the difference function $s1(z) = s(z) - s_{lin}$.

The s(z) is the vertical profile of a parameter, for example u at gridpoint i,j (see Fig. 4.3). s_{lin} is the linear function of regression determined by the six last values above the surface. s_{lin} represents the vertical gradient of s(z) at the boundary properly. This is especially for the temperature gradient very important, otherwise the diffusion would generate artificial buoyancy which finally implies artificial motion at the obstacle.

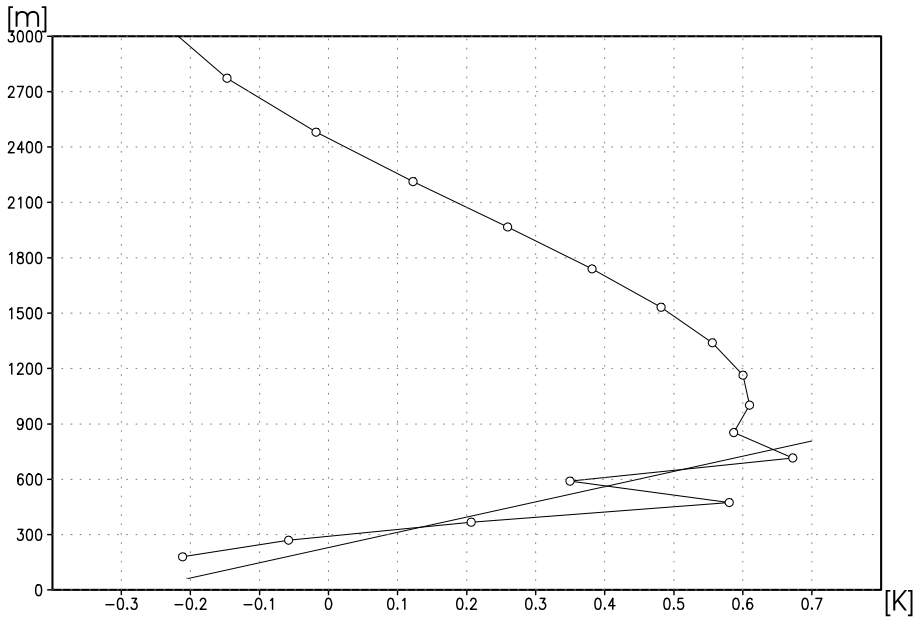

FIGURE 4.3: Vertical profile of the u-velocity with linear regression function.

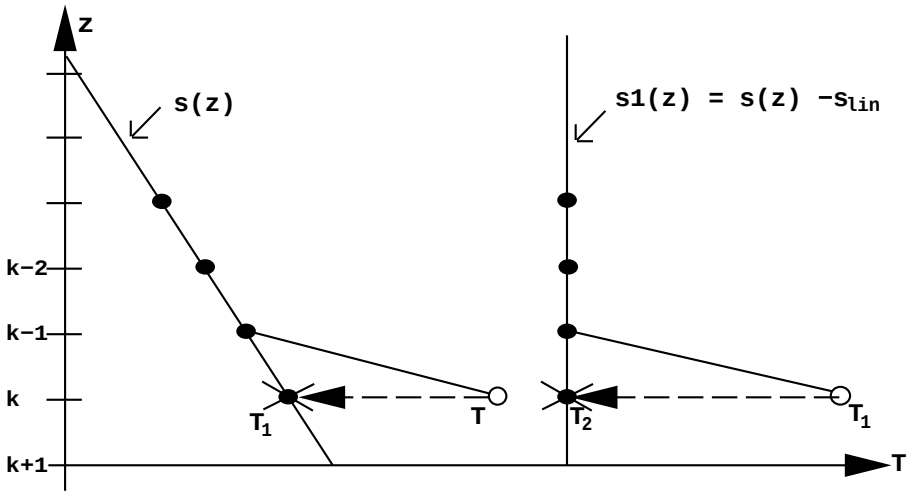

FIGURE 4.5: Action of diffussion for a temperature profile.

Fig. 4.4 shows a linear temperature profile s(z). The corresponding difference function s1(z) = s(z) - s_{lin} is represented on the right side of Fig. 3.4. Applying equation (3.5) for the vertical diffusion an s1(z) yields Δs_2 = s1(k-1) -s1(k-2) = 0 zsten in equation (3.5) is negativ and T_1 in Fig. 3.4 (right side) is nudged towards T_2. Since $\Delta s_2 = 0$ this demands $\Delta s_1 = 0$ if zsten should be 0. Δs_1 = s1(k)-s1(k-1)=0 this imlpies s1(k) = s1(k-1) in the equlibrium state when T_1 equals T_2. With this construction of the vertical diffusion the value T (Fig. 3.4, left side) is nudged towards T_1 which fits well into the vertical temperature distribution and in this way the vertical diffusion does not disturb an established vertical gradient. One particularity of the vertical diffusion has to be mentioned here: The diffusion coefficient is

decaying rapidly with height. Actually we need the diffusion right at the boundary rather than in the free flow domain. The existence of the vertical diffusion is absolutly necessary. One can drop horizontal diffusion rather than vertical diffusion at the boundary.

5 Results for Idealized Test Cases

The ability of the shaved element method can be tested on idealized experiments. The results presented below are carried out with a Gaussian mountain of $h_0 = 400$ m top height. The half width is set to $a = 10$ km. Since $\Delta x = 2$ km there are $5\Delta x$ to cover the half width. Thus the mountain is well resolved by sufficient gridpoints. The formula of the topography reads:

$$h(x,y) = \frac{h_0}{1 + \frac{x^2+y^2}{a^2}} \tag{91}$$

h_0	=	$400m$	top height of mountain
a	=	$10000m$	half width of mountain
u_0	=	$10\mathrm{m/s}$	basic current.

The temperature lapse rate corresponds to an atmospheric stability $N = 0.01\ s^{-1}$. The Scorer number

$$s_c = \frac{N}{u_0} a \tag{92}$$

is in this case equal to 10, which means the horizontal scale of the mountain is much larger than the horizontal wave length of the buoyancy oscillation and the nonhydrostatic effect is small. Thus the results represents the almost hydrostatic case. For small amplitude mountains $\left(\frac{Nh_0}{u_0} << 1\right)$ the steady linear solution is known. The following solutions of the shaved element experiments are verified against the steady solution of the LM-operational version with terrain following coordinates. Of course the results have to be interpolated on the same z-levels which are used for the shaved element experiments, in order to yield a valid comparison. In all the experiments the uniform basic flow is from left to right with 10 m/s. All the experiments show the steady state solution.

Fig. 5.1 shows the u-velocity in a vertiacl cross section (x-z-plane). The plane cuts the mountain through it's centre. The numbers at the contour lines are given in m/s. The flow is decelerated upstream of the mountain and accelerated in the lee, which is realistic. There is no windshadow detectable. No artificial vorticity modification is necessary in order to gain this solution. In Fig. 5.2 the same solution is represented, but here processed with the LM operational version with the terrain following coordinate system. On the first glance glance one cannot detect any difference. If we look in detail we find an additional contour line in Fig. 5.2 at the right side of the plot in lower parts and in upper levels the 10.3 m/s contour line (right half of plot) is a little bit more extended than in the shaved element plot.

Fig. 5.3 and Fig. 5.4 illustrate the vertical velocity w of the shaved element method and the terrain following system respectively. Again the two plots are almost congruent. Small differencies are visible when we look at the - 0.35 m/s contour line in lower levels. The area of the minimum vertical velocity is a little bit larger in the shaved element experiment. One can see the same phnomena in upper levels with the - 0.15 m/s contour line.

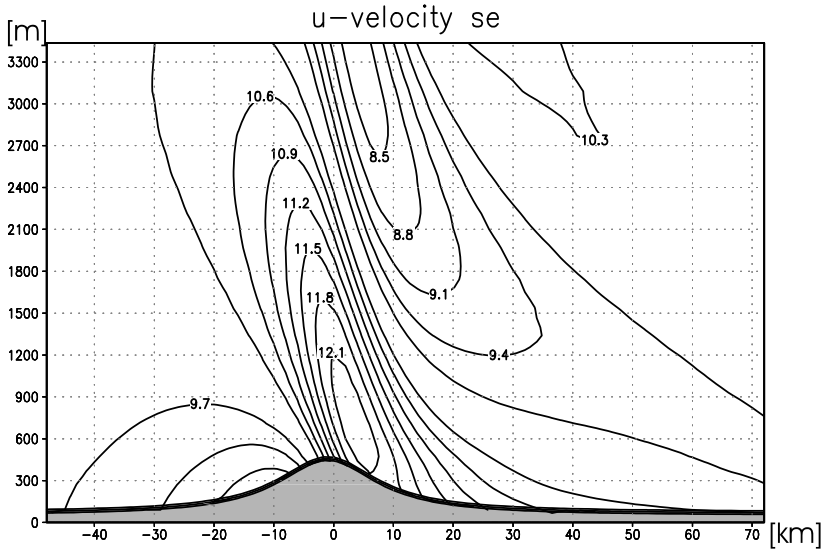

FIGURE 5.1: U-velocity in a vertical cross section computed by shaved elements.

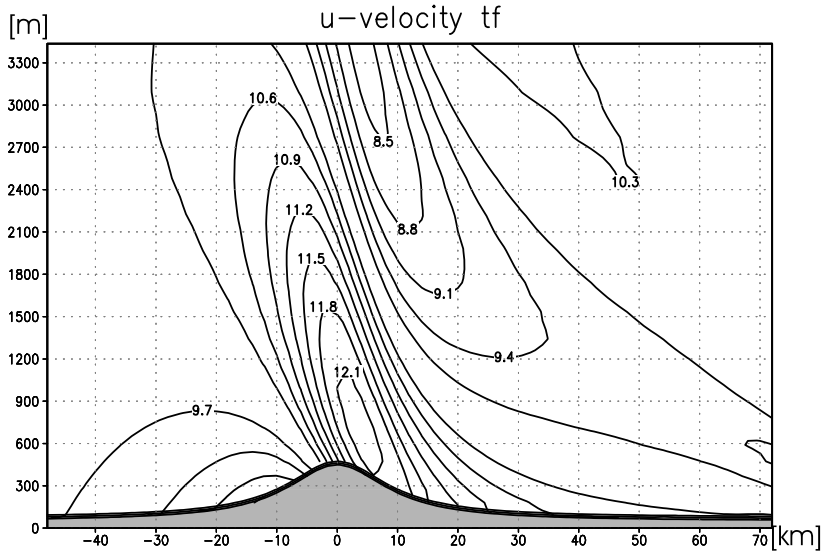

FIGURE 5.2: As in Fig. 5.1, but using the terrain following version of LM.

In Fig. 5.5 and 5.6 the vertical velocity is illustrated in a horizontal cross section at level z = 1164 m for both the shaved element experiments (Fig. 4.5) and the terrain following run (Fig. 5.6). There is no difference detectable.

Fig. 5.7 illustrates a vertical temperature profile which is the temperature deviation of the reference atmosphere (here shaved element experiment). The curvature of the profile in the lowest levels is remarkable. This means, the current model is able to simulate an inversion if the strongly bended profile is resolved with a few gridpoints. If the inversion is the represented just by one gridpoint, the vertical diffusion would act on it. From the mathematical point of view it would not make any sense to demand a resolution just by one gridpoint!

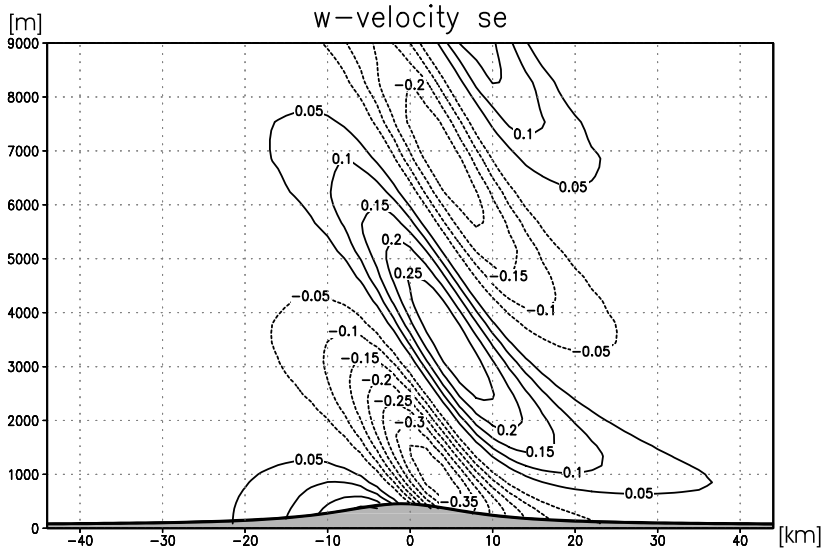

FIGURE 5.3: Vertical velocity in a vertical cross section computed by shaved elements.

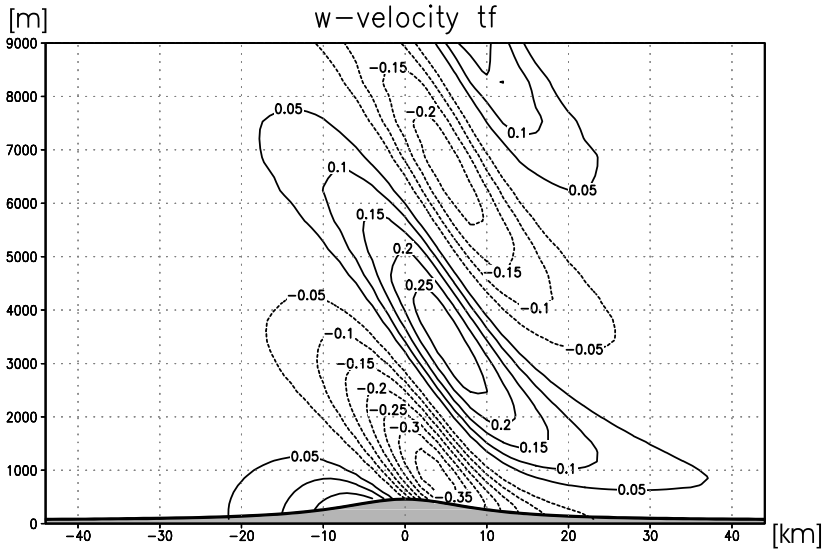

FIGURE 5.4: As in Fig. 5.3 but using the terrain following version of LM.

6 Summary

The new z-coordinate dynamical core of the LM has been described in detail. This version allows for a better orography representation by avoiding the forcing of the atmosphere by numerical errors in the presence of mountains. Problems concerning the prediction of precipitation which have been discussed in the literature in connection with similar approaches are solved by introducing a simplified version of the shaved element finite volume method using the thin wall approximation.

In this approach the mountains are represented by continuous linear splines. A regular grid is cut by this orographic function, which near the surface produces cut cells of different size and shape, which are treated by the finite volume method. For cells not cut by the orographic function the finite volume method produces the finite difference scheme of the operational

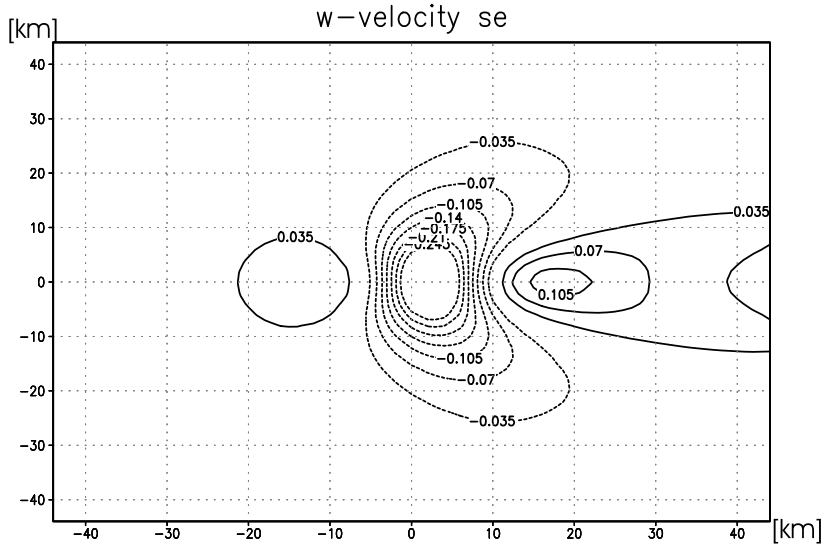

FIGURE 5.5: Vertical velocity in a horizontal cross section computed by shaved elements.

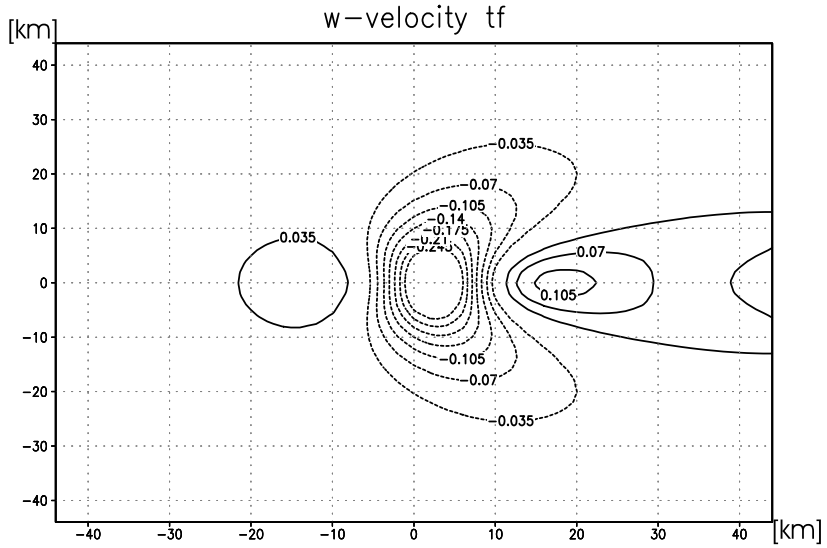

FIGURE 5.6: As in Fig. 5.5, but for the LM with terrain following coordinate.

LM, specialized for the case of flat terrain. The finite difference equations are based on centred difference approximation on the C-grid for those elements which are not cut by the topographic function. For the elements cut by the topographic function the finite difference equations are formulated using flux limiters in the horizontal and vertical directions. A small amount of numerical smoothing is required to stabilize the Leapfrog time-integration scheme.

A number of three-dimensional numerical tests have been performed with the new dynamical core. They showed that the method developed does not suffer from the problems reported in connection with the $\eta-$coordinate (Mesinger, 1988). Especially, the solutions for hydrostatic flow over a bell shaped-smooth mountain are rather similar to those obtained by a terrain following version of the model. Future work will focus on the inclusion of physical paramterizations to allow testing for real cases, aiming at an operational application of the z-coordinate version of the LM.

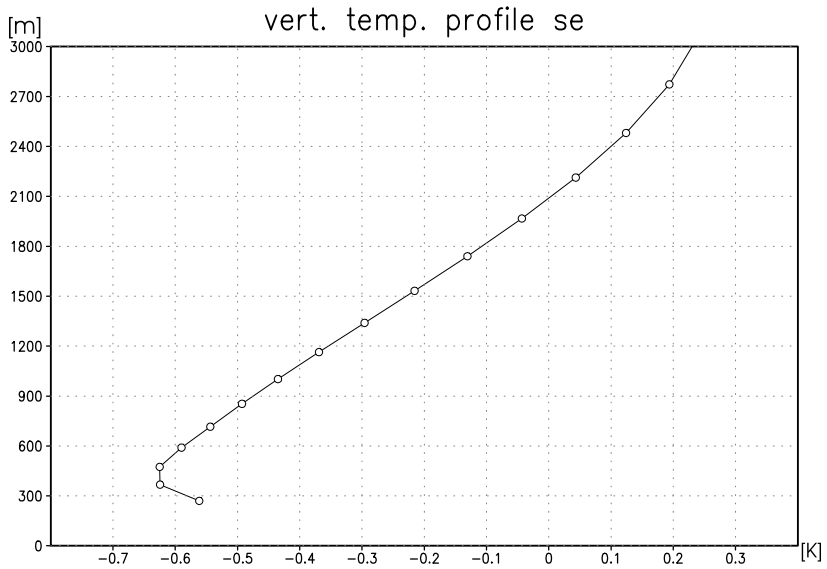

FIGURE 5.7: A vertical temperature profile simulated by shaved elements.

References

Doms, G. and U. Schättler, 1999: The Nonhydrostatic Limited Area Model LM. Part I: Scientific Documentation, DWD (available at www.cosmo-model.org).

Appendix

The following variable are used as substitutes / abbreviations for complex assembled expressions:

$$\frac{\overline{\rho_o}^{h\zeta}}{\overline{\rho^n}^{h\zeta}} = \frac{(\rho_0)_{k-1/2}}{(\rho^n)_{k-1/2}} = \frac{(\Delta p_0)_{k-1}(\rho_0)_k + (\Delta p_0)_k (\rho_0)_{k-1}}{(\Delta p_0)_{k-1}\rho_k^n + (\Delta p_0)_k \rho_{k-1}^n} \tag{93}$$

$$\begin{aligned}\frac{\overline{\rho_o}^{h\zeta}}{\overline{\rho^n}^{h\zeta}}\overline{A}^{h\zeta} &= \frac{(\rho_0)_{k-1/2}}{(\rho^n)_{k-1/2}}A_{k-1/2} = \frac{1}{(\Delta p_0)_{k-1} + (\Delta p_0)_k} \\ &\quad \frac{(\Delta p_0)_{k-1}(\rho_0)_k + (\Delta p_0)_k(\rho_0)_{k-1}}{(\Delta p_0)_{k-1}\rho_k^n + (\Delta p_0)_k \rho_{k-1}^n} \\ &\quad \left((\Delta p_0)_{k-1} A_k + (\Delta p_0)_k A_{k-1}\right)\end{aligned} \tag{94}$$

$$\frac{\overline{\rho_o}^{h\zeta}}{\overline{\rho^n}^{h\zeta}}\overline{A}^{h\zeta} = y_{k-1/2}\left((\Delta p_0)_{k-1} A_k + (\Delta p_0)_k A_{k-1}\right) \tag{95}$$

$$y_{k-1/2} = \frac{1}{(\Delta p_0)_{k-1} + (\Delta p_0)_k}\frac{(\Delta p_0)_{k-1}(\rho_0) + (\Delta p_0)_k(\rho_0)_{k-1}}{(\Delta p_0)_{k-1}\rho_k^n + (\Delta p_0)_k\rho_{k-1}^n} \tag{96}$$

$$\frac{1}{(\Delta p_0)_{k-1/2}}\frac{\overline{\rho_o}^{h\zeta}}{\overline{\rho^n}^{h\zeta}} = 2y_{k-1/2} \tag{97}$$

$$x_k = \left(\frac{T_0}{T^n p_0}\right)_k \tag{98}$$

$$s_k^\nu = \left(\frac{T^\nu - T_0}{T^n}\right)_k \tag{99}$$

$$C_{k-1/2}^{w1} = 2g\Delta\tau y_{k-1/2} \tag{100}$$

$$\alpha_{k-1/2}^B = 1 - (\Delta p_0)_{k-1}\frac{1}{2}x_k \tag{101}$$

$$\alpha_{k-1/2}^T = 1 + (\Delta p_0)_k \frac{1}{2}x_{k-1} \tag{102}$$

$$C_k^{p1} = \frac{g(\rho_0)_k \Delta\tau}{(\Delta p_0)_k}\frac{p_k^n c_p}{c_v} \tag{103}$$

$$C_k^{p2} = \frac{g}{2}(\rho_0)_k \Delta\tau \tag{104}$$

From the temperature equation (2.27) we gain:

$$\begin{aligned} T_k^{\nu+1} &= T_k^\nu + R_k \qquad\qquad T_k^{\nu+1} - T_{0_k} = T_k^\nu - T_{0_k} + R_k \\ R_k &= \text{rest of right hand side of equation} \\ \frac{T_k^{\nu+1} - T_{0_k}}{T_k^n} &= \frac{T_k^\nu - T_{0_k}}{T_k^n} + \frac{R_k}{T_k^n} \\ s_k^{\nu+1} &= s_k^\nu + \frac{R_k}{T_k^n} \end{aligned} \tag{105}$$

$$
\begin{aligned}
s_k^{\nu+1} &= s_k^{\nu} + \frac{(f_T^n)_k \,\Delta\tau}{T_k^n} - \left(\frac{p_k^n}{\rho_k^n c_v}\right)\left(D_h^{\nu+1}\right)_k \frac{\Delta\tau}{T_k^n} + \frac{g\,(\rho_0)_k}{(\Delta p_0)_k}\frac{\Delta\tau}{T_k^n} \\
&\quad \frac{p_k^n}{\rho_k^n c_v}\beta^- \left(fxy_{k+1/2} w_{k+1/2}^{\nu} - fxy_{k-1/2} w_{k-1/2}^{\nu}\right) + \frac{g\,(\rho_o)_k}{(\Delta p_0)_k} \\
&\quad \frac{\Delta\tau}{T_k^n}\frac{p_k^n}{\rho_k^n c_v}\beta^+ \left(fxy_{k+1/2} w_{k+1/2}^{\nu+1} - fxy_{k-1/2} w_{k-1/2}^{\nu+1}\right) \qquad (106)
\end{aligned}
$$

$$
\begin{aligned}
\left((\Delta p_0)_{k-1}\frac{1}{2}s_k^{\nu+1} + (\Delta p_0)_k \frac{1}{2}s_{k-1}^{\nu+1}\right) &= C_{k-1/2}^T + \beta^+ (\Delta p_0)_{k-1} C_k^{T1} \\
&\quad \left(fxy_{k+1/2} w_{k+1/2}^{\nu+1} - fxy_{k-1/2} w_{k-1/2}^{\nu+1}\right) \\
&\quad +\beta^+ (\Delta p_0)_k C_{k-1}^{T1} \left(fxy_{k-1/2}\right. \\
&\quad \left. w_{k-1/2}^{\nu+1} - fxy_{k-11/2} w_{k-11/2}^{\nu+1}\right) \qquad (107)
\end{aligned}
$$

$$
\begin{aligned}
C_{k-1/2}^T &= (\Delta p_0)_{k-1}\frac{1}{2}s_k^{\nu} + (\Delta p_0)_k \frac{1}{2}s_{k-1}^{\nu} + (\Delta p_0)_{k-1}\frac{(f_T^n)_k\,\Delta\tau}{2T_k^n} + (\Delta p_0)_k \\
&\quad \frac{(f_T^n)_{k-1}\,\Delta\tau}{2T_{k-1}^n} + (\Delta p_0)_{k-1}\frac{zcpr_k}{2T_k^n}\left[-zpnj_k\left(D_h^{\nu+1}\right)_k + \beta^-\right. \\
&\quad \left. zcp1_k\left(fxy_{k+1/2} w_{k+1/2}^{\nu} - fxy_{k-1/2} w_{k-1/2}^{\nu}\right)\right] + (\Delta p_0)_k \\
&\quad \frac{zcpr_{k-1}}{2T_{k-1}^n}\left[-zpnj_{k-1}\left(D_h^{\nu+1}\right)_k + \beta^- zcp1_{k-1}\right. \\
&\quad \left.\left(fxy_{k-1/2} w_{k-1/2}^{\nu} - fxy_{k-11/2} w_{k-11/2}^{\nu}\right)\right] \qquad (108)
\end{aligned}
$$

with

$$
\begin{aligned}
zcpr_k &= \frac{1}{c_p \rho_k^n} \quad ; \quad zpnj_k = \frac{c_p}{c_v} p_k^n \Delta\tau \\
zcp1_k &= \frac{c_p}{c_v} p_k^n \Delta\tau\,(\rho_0)_k \frac{g}{(\Delta p_0)_k} \\
zcpr_k zcp1_k &= \frac{p_k^n \Delta\tau\,(\rho_0)_k\, g}{\rho_k^n c_v\,(\Delta p_0)_k} \quad \text{and} \quad c_k^{T1} = \frac{zcpr_k zcp1_k}{2T_k^n}
\end{aligned}
$$

List of COSMO Newsletters and Technical Reports

(available for download from the COSMO Website: www.cosmo-model.org)

COSMO Newsletters

Newsletter No.1, February 2001.

Newsletter No.2, February 2002.

COSMO Technical Reports

No. 1, Dmitrii Mironov and Matthias Raschendorfer (2001):
Evaluation of Empirical Parameters of the New LM Surface-Layer Parameterization Scheme. Results from Numerical Experiments Including the Soil Moisture Analysis.

No. 2, Reinhold Schrodin and Erdmann Heise (2001):
The Multi-Layer Version of the DWD Soil Model TERRA_LM.

No. 3, Günther Doms (2001):
A Scheme for Monotonic Numerical Diffusion in the LM.

No. 4, Hans-Joachim Herzog, Ursula Schubert, Gerd Vogel, Adelheid Fiedler and Roswitha Kirchner (2002):
LLM – the High-Resolving Nonhydrostatic Simulation Model in the DWD – Project LITFASS. Part I: Modelling Technique and Simulation Method.

No. 5, Jean-Marie Bettems (2002):
EUCOS Impact Study Using the Limited-Area Non-Hydrostatic NWP Model in Operational Use at MeteoSwiss.

No. 6, Heinz-Werner Bitzer and Jürgen Steppeler (2004):
Documentation of the Z-Coordinate Dynamical Core of LM.

COSMO Technical Reports

Issues of the COSMO Technical Reports series are published by the *Consortium for Small-Scale Modelling* at non-regular intervals. COSMO is a European group for numerical weather prediction with participating meteorological services from Germany (DWD, AWGeophys), Greece (HNMS), Italy (UGM, ARPA-SMR) and Switzerland (MeteoSwiss). The general goal is to develop, improve and maintain a non-hydrostatic limited area modelling system to be used for both operational and research applications by the members of COSMO. This system is initially based on the Lokal-Modell (LM) of DWD with its corresponding data assimilation system.

The Technical Reports are intended

- for scientific contributions and a documentation of research activities,
- to present and discuss results obtained from the model system,
- to present and discuss verification results and interpretation methods,
- for a documentation of technical changes to the model system,
- to give an overview of new components of the model system.

The purpose of these reports is to communicate results, changes and progress related to the LM model system relatively fast within the COSMO consortium, and also to inform other NWP groups on our current research activities. In this way the discussion on a specific topic can be stimulated at an early stage. In order to publish a report very soon after the completition of the manuscript, we have decided to omit a thorough reviewing procedure and only a rough check is done by the editors and a third reviewer. We apologize for typographical and other errors or inconsistencies which may still be present.

At present, the Technical Reports are available for download from the COSMO web site (www.cosmo-model.org). If required, the member meteorological centres can produce hard-copies by their own for distribution within their service. All members of the consortium will be informed about new issues by email.

For any comments and questions, please contact the editors:

Günther Doms
guenther.doms@dwd.de

Ulrich Schättler
ulrich.schaettler@dwd.de